

First-order condensation transition in the position distribution of a run-and-tumble particle in one dimension

Francesco Mori,¹ Giacomo Gradenigo,^{2,3} and Satya N. Majumdar¹

¹*LPTMS, CNRS, Univ. Paris-Sud, Université Paris-Saclay, 91405 Orsay, France*

²*Gran Sasso Science Institute, Viale F. Crispi 7, 67100 L'Aquila, Italy*

³*INFN-Laboratori Nazionali del Gran Sasso, Via G. Acitelli 22, 67100 Assergi (AQ), Italy*

(Dated: April 24, 2022)

We consider a single run-and-tumble particle (RTP) moving in one dimension. We assume that the velocity of the particle is drawn independently at each tumbling from a zero-mean Gaussian distribution and that the run times are exponentially distributed. We investigate the probability distribution $P(X, N)$ of the position X of the particle after N runs, with $N \gg 1$. We show that in the regime $X \sim N^{3/4}$ the distribution $P(X, N)$ has a large deviation form with a rate function characterized by a discontinuous derivative at the critical value $X = X_c > 0$. The same is true for $X = -X_c$ due to the symmetry of $P(X, N)$. We show that this singularity corresponds to a first-order condensation transition: for $X > X_c$ a single large jump dominates the RTP trajectory. We consider the participation ratio of the single-run displacements as the order parameter of the system, showing that this quantity is discontinuous at $X = X_c$. Our results are supported by numerical simulations performed with a constrained Markov chain Monte Carlo algorithm.

I. INTRODUCTION

Active systems, characterized by the ability to convert energy from the environment into persistent motion, are ubiquitous in nature. Examples of active matter include flocking of birds [1–3], active gels [1, 4] and self-propelled bacteria [5–7]. The persistent motion of their components drives these systems out-of-equilibrium, giving rise to a wide range of fascinating phenomena. Even though several of these features arise from the complex interactions of several components [5, 6, 8, 9], many interesting phenomena, e.g., the universality of the survival probability [10–12], can be already observed at the single-particle level, where one can often obtain exact analytical results.

One of the most studied models of active matter is the run-and-tumble particle (RTP). This model was originally known as persistent random walk [13–18] and has been applied in recent years to describe the directed motion of a class of bacteria, including *E. Coli* [5–8, 19]. These bacteria typically move alternating between running phases of straight motion with constant velocity, to tumblings, i.e., sudden changes of direction. Despite its apparent simplicity, this model encapsulates several general features of active matter, including motility-induced phase separation [8] and non-Boltzmann steady states in the presence of a confining potential [5, 20–23].

One of the simplest and most natural observables that one can investigate for the RTP model in one dimension is the probability density function (PDF) $P(X, N)$ of the position X of a single RTP after N running phases [14, 24–29]. For the RTP model and its many variants, computing $P(X, N)$ for any N is usually nontrivial. Note that, if the initial velocity is chosen at random, the PDF $P(X, N)$ is symmetric around $X = 0$, i.e. $P(X, N) = P(-X, N)$. For $N \gg 1$, as a consequence of the central limit theorem (CLT), one expects $P(X, N)$ to be Gaussian in the region $|X| \sim \sqrt{N}$ [6]. However, out-

side the range of validity of the CLT, i.e., for $|X| \gg \sqrt{N}$, the shape of $P(X, N)$ depends on the details of the model and is usually not Gaussian. The large-deviation tails of $P(X, N)$ have been studied for a large class of RTP models [25–29], including RTPs moving in d dimensions (for which X represents the x -component of the position of the particle) [28, 29] and RTP models for which the speed v of the particle during each running phase is drawn from some distribution $W(v)$ [26, 29]. In particular, it has been shown that, under certain conditions [29], the system undergoes a condensation phase transition at some critical value X_c of the position X [29]. Below the transition, the different running phases contribute to the total displacement X by roughly the same amount. Conversely, for $|X| > X_c$, a single running phase, called *condensate*, dominates the trajectory, contributing to a finite fraction of X (see the insets in Fig. 1). This condensation transition leads to a non-analytic behavior of the PDF $P(X, N)$ at the critical points $X = \pm X_c$ (see Fig. 1).

In the vicinity of the transition, the PDF $P(X, N)$ can be written as

$$P(X, N) \simeq \exp \left[-N^{2\alpha-1} F \left(\frac{X}{N^\alpha} \right) \right], \quad (1)$$

where $F(z)$ is the rate function associated to the large-deviation regime and the exponent $\alpha > 0$, that depends on the model, determines the scale of the large deviations. Notably, the dynamical phase transition is signaled by the non-analyticity of $F(z)$ at the critical point $z = z_c$, where $z_c = X_c/N^\alpha$. In particular, the transition is said to be of order n if the n -th derivative of $F(z)$ is discontinuous at $z = z_c$. For instance, in Ref. [29], it was shown that for an RTP in d dimensions and for a family on the speed distributions $W(v)$ the system undergoes a transition of order $n \geq 2$, where n depends on the system parameters. Similarly, in Ref. [26] a one-dimensional RTP in the presence of a constant drive $E > 0$ and with

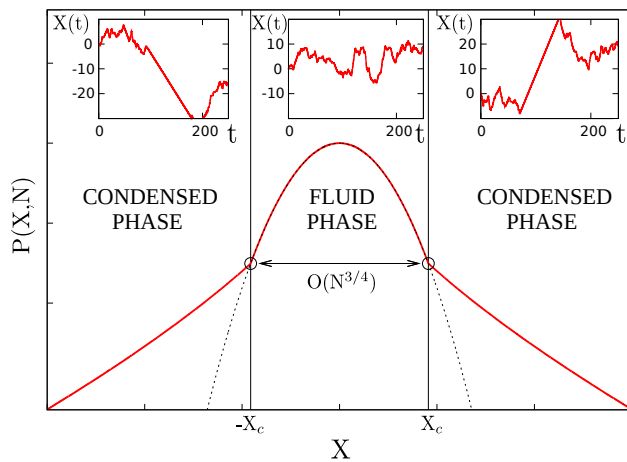


FIG. 1. *Main*: Schematic representation of the PDF $P(X, N)$ of the final position X of a single run-and-tumble particle (RTP) after $N \gg 1$ running phases. The central region $-X_c < X < X_c$ [with $X_c \sim O(N^{3/4})$] describes the fluid phase where $P(X, N)$ has a Gaussian shape. For $X > X_c$ (and by symmetry for $X < -X_c$) the system is in the condensed phase, where $P(X, N)$ has an anomalous shape. *Insets*: Typical RTP trajectories $X(t)$ as a function of the time t . In the condensed phase (external panels), the trajectory is dominated by a single run. In the fluid phase (central panel), the runs contribute to the total displacement by roughly the same amount

Gaussian speed distribution $W(v)$ was considered. In this case, it was shown that the system undergoes a first-order phase transition, i.e., $n = 1$. However, it was not clear whether a first-order transition could be observed for an RTP system without an external drive. Moreover, it is also relevant to ask whether or not this first-order dynamical phase transition is associated with a discontinuity of some order parameter, as observed for equilibrium phase transitions.

In addition to RTP systems, this kind of real-space condensation transitions has been observed in a wide range of situations [30, 31]. Examples include the discrete nonlinear Schrödinger equation [32–36], economic and financial models [37–39], and mass-transport models [40–48]. In these systems, a phase transition is observed when a control parameter, e.g., the total mass of the system [40] or the total energy [34], is increased above a critical threshold. Above this critical point, a condensate appears in real space absorbing a macroscopic fraction of the total mass. For instance, in the context of mass-transport models on lattices the condensate is a single lattice site carrying a finite fraction of the total mass. Similarly, in the context of wealth distribution in a population, the analogous of a condensate would be an extremely wealthy individual. In the case of RTPs the condensate is a single running phase which dominates the trajectory.

In this paper, we consider a single RTP on a line. We choose the velocity distribution $W(v)$ to be Gaussian and

the distribution of the time between two tumblings to be exponential. We investigate the distribution $P(X, N)$ of the position of the particle in the late-time limit. We show that in the large-deviation regime where $X \sim N^{3/4}$, corresponding to $\alpha = 3/4$ in Eq. (1), the particle undergoes a first-order phase transition and we compute exactly the corresponding rate function $F(z)$. Moreover, we provide a detailed description of the mechanism of this transition. We identify the relevant order parameter for the system, showing that it undergoes a jump discontinuity at $z = z_c$. We also verify our results by performing high-precision numerical simulations. This RTP model corresponds to the one considered in Ref. [26] but with no external drive ($E = 0$). Note that $E = 0$ is a singular point in the sense that the scale at which the transition occurs and the mechanism of the transition for $E > 0$ [26] are different in the $E = 0$ case studied here.

The rest of the paper is organized as follows. In Section II we provide the details of the model and we present a summary of the salient results. The details of the computation of the late-time position distribution of the RTP are presented in Sec. III. In Section IV, we investigate the marginal probability distribution of the displacement of the RTP during a single running phase and we identify the relevant order parameter of the system. Finally, in Section V we conclude with a summary of the paper and few remarks. Some details of the computations and of the numerical simulations are presented in the Appendices.

II. THE MODEL AND THE SUMMARY OF THE MAIN RESULTS

A. The model

We consider a single RTP on a line, starting initially at the origin. The particle chooses a velocity v_1 (positive or negative), drawn from the distribution $W(v)$, and starts to move with constant velocity v_1 . After some time τ_1 , drawn from the time distribution $p(\tau)$, the particle tumbles, i.e., it chooses a new velocity v_2 , independently drawn from $W(v)$. Then, it starts moving with the new velocity v_2 , until it tumbles again after some random time τ_2 , drawn from $p(\tau)$. We assume that the tumblings happen instantaneously and that the running times are drawn from an exponential distribution with average value $1/\gamma$, i.e., that

$$p(\tau) = \gamma \exp(-\gamma\tau)\theta(\tau) \quad (2)$$

where $\theta(\tau)$ is the Heaviside theta function, i.e., $\theta(\tau) = 1$ for $\tau \geq 0$ and $\theta(\tau) = 0$ for $\tau < 0$. The parameter γ is the tumbling rate of the RTP. Moreover, we assume that the velocity distribution is Gaussian with zero mean and variance σ^2 . In other words, we choose

$$W(v) = \frac{1}{\sqrt{2\pi}\sigma} \exp[-v^2/(2\sigma^2)]. \quad (3)$$

For the sake of simplicity, we set $\sigma^2 = \gamma = 1$ in the rest of the paper.

When considering the RTP model, one can either observe a trajectory up to some fixed time T (*fixed-T ensemble*) or until N running phases are completed (*fixed-N ensemble*). Accordingly, one either studies the PDF $P(X, T)$ of the position X of the RTP after time T or the PDF $P(X, N)$ of X after N running phases. In Ref. [29] it was shown that the late time behavior is qualitatively similar for the two ensembles. Since performing the computation is technically easier at fixed N , for the sake of simplicity we focus here on the fixed- N ensemble. Our results can be generalized to the fixed- T case. The total displacement of the particle after N runs is given by

$$X = \sum_{i=1}^N x_i, \quad (4)$$

where $x_i = v_i \tau_i$ is the displacement during the i -th running phase. The velocities v_1, \dots, v_N are independent and identically distributed (i.i.d.) random variables drawn from the PDF in Eq. (3). Similarly, the times τ_1, \dots, τ_N are i.i.d. exponentially distributed random variables with rate γ .

Thus, the distribution of a single-run displacement x_i is given by

$$\mathcal{P}(x) = \int_{-\infty}^{\infty} dv \int_0^{\infty} d\tau W(v) p(\tau) \delta(x - v\tau). \quad (5)$$

Using the expressions for $p(\tau)$ and $W(v)$ given in Eqs. (2) and (3) respectively, one obtains

$$\mathcal{P}(x) = \frac{1}{\sqrt{2\pi}} \int_0^{\infty} d\tau \frac{1}{\tau} e^{-\tau - x^2/(2\tau^2)}. \quad (6)$$

It turns out that this expression can be written in terms of the Meijer G-function $G_{0,3}^{3,0}(x|\dots)$, which can be evaluated using Mathematica, as

$$\mathcal{P}(x) = \frac{1}{2\sqrt{2\pi}} G_{0,3}^{3,0} \left(x^2/8 \left| \begin{array}{ccc} 0 & 0 & 0 \\ 0 & 0 & 1/2 \end{array} \right. \right). \quad (7)$$

From this expression in Eq. (7) we observe that the marginal distribution $\mathcal{P}(x)$ is symmetric around $x = 0$. The mean and the variance of $x = v\tau$ can be easily computed. While the mean is simply

$$\langle x \rangle = 0, \quad (8)$$

the variance reads

$$\langle x^2 \rangle - \langle x \rangle^2 = \langle v^2 \rangle \langle \tau^2 \rangle = 2. \quad (9)$$

From the expression for the marginal distribution $\mathcal{P}(x)$ in Eq. (6) one can show that when $|x| \rightarrow \infty$ (see Appendix A)

$$\mathcal{P}(x) \approx \frac{1}{\sqrt{3}|x|^{1/3}} e^{-3|x|^{2/3}/2}. \quad (10)$$

Thus the jump distribution $\mathcal{P}(x)$ has a stretched exponential tail $\sim \exp[-(3/2)|x|^{2/3}]$. Notably, the single-run PDF $\mathcal{P}(x)$ satisfies the condition for condensation presented in Ref. [29]. This criterion was derived using a grand canonical argument and states that if the PDF $\mathcal{P}(x)$ satisfies

$$e^{-c|x|} < \mathcal{P}(x) < 1/|x|^3 \quad (11)$$

for large $|x|$, where $c > 0$ is any positive constant, then the corresponding RTP model displays a condensation transition. Since the PDF in Eq. (10) satisfies the condition in Eq. (11), we expect that the system undergoes a dynamical phase transition in the large-deviation regime of X .

In Ref. [29] a detailed analysis of the condensation transition was carried out in the case where $\mathcal{P}(x)$ has a power-law tail for large $|x|$. The main goal of this paper is instead to investigate the case where $\mathcal{P}(x)$ has a stretched exponential tail, for which both the scale and the mechanism of the phase transition are different from the power-law case. In particular, in the stretched-exponential case the size of the condensate scales as $N^{3/4}$ and the transition is first-order. Conversely, in the model studied in [29], the condensate mass scales linearly in N and the transition is of order $n \geq 2$.

Note that the case where $\mathcal{P}(x)$ has a stretched exponential tail has also been studied in the context of the discrete nonlinear Schrödinger equation [34–36]. However, in that case the distribution $\mathcal{P}(x)$ has support only for positive x and the phase transition occurs at a different scale, namely for $X \sim O(N)$. In this paper instead the variable x can be positive or negative and $\mathcal{P}(x)$ is symmetric around $x = 0$.

Given the marginal distribution $\mathcal{P}(x)$ in Eq. (5) for the displacements x_1, \dots, x_N , we are interested in computing the PDF $P(X, N)$ of the final position $X = \sum_{i=1}^N x_i$. Since the displacements x_1, \dots, x_N are i.i.d. random variables, their joint probability distribution is simply given by the product of the marginal probabilities, and we obtain

$$P(X, N) = \prod_{i=1}^N \int_{-\infty}^{\infty} dx_i \mathcal{P}(x_i) \delta \left(X - \sum_{i=1}^N x_i \right), \quad (12)$$

where the delta function enforces the final position to be X and $\mathcal{P}(x)$ is given in Eq. (5).

It is clear from Eq. (12) that studying the distribution of X simply amounts to the classical problem of finding the distribution of the sum of N i.i.d. random variables, each drawn from the symmetric distribution $\mathcal{P}(x)$. This problem has been extensively investigated in the probability literature [49] and has recently been studied for correlated variables [50]. In particular, the case where $\mathcal{P}(x)$ has stretched exponential tails $\mathcal{P}(x) \sim e^{-a|x|^\beta}$, with $a > 0$ and $0 < \beta < 1$ was first investigated by Nagaev [51, 52], who identified the presence of a non-trivial large deviation regime of $P(X, N)$ in the region

$|X| \sim N^{1/(2-\beta)}$. Note that our RTP model corresponds to $a = 3/2$ and $\beta = 2/3$. Moreover, the rate function associated to this large-deviation regime was derived for any $\beta > 0$ in a recent mathematical work [53]. In this paper, we present an alternative derivation of the rate function $F(z)$, which is in agreement with the result of Ref. [53] (see appendix G). In addition, we provide a detailed analysis of the mechanism of the phase transition, investigating the marginal probability distribution of a single-run displacement and identifying the order parameter associated to the transition, which were not addressed in Ref. [53].

B. The summary of the main results

Since the detailed derivations are somewhat technical, it is useful to provide a summary of the salient features of our main results. This is the purpose of this section, while the detailed derivations are presented in the following sections. We provide a threefold description of the dynamical phase transition, based on the analysis of three main observables: (1) the position distribution of the particle, (2) the marginal probability of a single-run displacement, and (3) the participation ratio, i.e., the order parameter associated to the condensation transition.

1. Position distribution

Our first goal is to investigate the distribution $P(X, N)$ of the position X of the RTP after N running phases. In the limit of large N we identify three distinct regimes. In the typical regime $|X| \sim \sqrt{N}$, the distribution of X is Gaussian,

$$P(X, N) \sim e^{-X^2/4}, \quad (13)$$

as a consequence of the CLT. On the other hand, in the large-deviation regime where X scales linearly in N , i.e., $|X| \sim N$, we find that the final position is dominated by a single large displacement, a phenomenon also observed in the recent literature on anomalous transport [50, 54–56]. Thus, in this region the PDF of X can be written as

$$P(X, N) \simeq N\mathcal{P}(X), \quad (14)$$

where $\mathcal{P}(x)$ is the single-run PDF, given in Eq. (7), and the factor N comes from the fact that any of the N i.i.d. displacements can be the condensate. Thus, for $|X| \sim N$, $P(X, N)$ has a stretched exponential tail [see Eq. (10)]

$$P(X, N) \sim e^{-(3/2)|X|^{2/3}}. \quad (15)$$

To identify the correct scale at which the crossover between these two regimes occurs we match the Gaussian

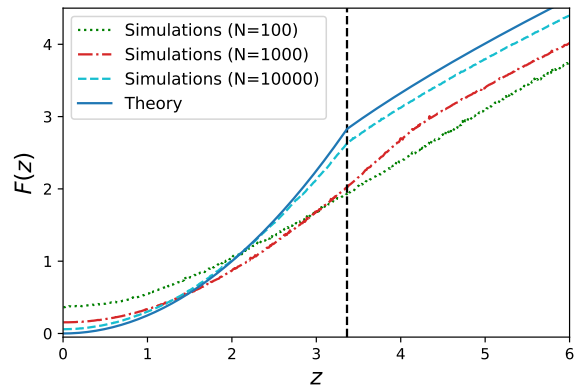


FIG. 2. The rate function $F(z)$ versus $z = X/N^{3/4}$. The continuous blue line represents the theoretical result in Eq. (18), while the dashed lines depict the results of numerical simulations, for different values of N . The first derivative of $F(z)$ is discontinuous at the critical point $z_c = 2^{7/4}$, marked by a dashed vertical line.

weight in Eq. (13) with the stretched-exponential tail in Eq. (15)

$$e^{-X^2/4} \sim e^{-(3/2)|X|^{2/3}}, \quad (16)$$

yielding $|X| \sim N^{3/4}$. Thus, we zoom in this region $|X| \sim N^{3/4}$ and set $X = zN^{3/4}$, where z describes the scaled position in the vicinity of the transition. In this intermediate regime, the distribution of X assumes an anomalous large-deviation form. We observe that the PDF $P(X, N)$ is described by a Gaussian probability weight up to some critical value $X_c = z_c N^{3/4}$ (where z_c is a constant of order one), far outside of the region predicted by the CLT. At this critical point, the system undergoes a first-order condensation transition, signaled by a discontinuity in the first derivative of the rate function $F(z)$, where $z = X/N^{3/4}$.

These different regimes can be summarized as follows

$$P(X, N) \approx \begin{cases} \exp\left[-\frac{X^2}{4N}\right] & \text{for } |X| \sim \sqrt{N}, \\ \exp\left[-\sqrt{N}F\left(\frac{|X|}{N^{3/4}}\right)\right] & \text{for } |X| \sim N^{3/4}, \\ \exp\left[-\frac{3}{2}|X|^{2/3}\right] & \text{for } |X| \sim N, \end{cases} \quad (17)$$

where

$$F(z) = \begin{cases} z^2/4 & \text{for } z < z_c, \\ \chi(z) & \text{for } z > z_c, \end{cases} \quad (18)$$

with $z_c = 2^{7/4}$. Note that, for $z < z_c$, $P(X, N)$ is still described by the same Gaussian weight as in the typical regime. The function $\chi(z)$ can be computed only in the

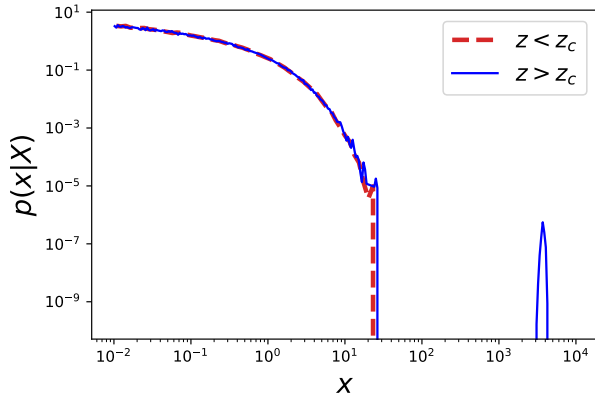


FIG. 3. Marginal probability $p(x|X)$ of a single-run displacement as a function of x , obtained from numerical simulations with $N = 10^4$. The dashed red line corresponds to numerical simulations performed in the fluid phase, for $z < z_c$, where $z = X/N^{3/4}$. For $z > z_c$ (continuous blue line) the system is in the condensed phase and a bump appears in the tail of $p(x|X)$.

region $z > z_\ell = 4(2/3)^{3/4}$. Luckily, it turns out that $z_\ell = 2.9511\dots < z_c = 3.3635\dots$ and thus we find the exact expression of $\chi(z)$ in the region of interest $z > z_c$. The full expression of $\chi(z)$ is rather complicated and is given in Eq. (C10) of Appendix C. Its asymptotic behavior is given by

$$\chi(z) = \begin{cases} \sqrt{6} + o(1) & \text{when } z \rightarrow z_\ell, \\ \frac{3}{2}z^{2/3} - z^{-2/3} + o(z^{-2/3}) & \text{when } z \rightarrow \infty. \end{cases} \quad (19)$$

From the second line of Eq. (19) we observe that the rate function can be approximated as $F(z) \simeq (3/2)z^{2/3}$ for large z , smoothly connecting to the extreme large deviation regime [see the third line of Eq. (17)]. From Eq. (18), we observe that the rate function $F(z)$ is singular at the critical point $z = z_c$. Since the first derivative of $F(z)$ is discontinuous at $z = z_c$, we say that the system undergoes a first-order phase transition at $z = z_c$. The exact result for the rate function $F(z)$ is shown in Fig. (2) (continuous blue line), and is in good agreement with numerical simulations (dotted lines), performed with a constrained Markov chain Monte Carlo (MCMC) algorithm (for the details of the numerics see Appendix B).

2. Marginal probability distribution of a single-run displacement

To gain insights into the nature of this first-order transition, we present a detailed study of the marginal probability distribution $p(x|X)$ of a single displacement conditioned on the total displacement X . This variable x can be any of the displacements x_1, \dots, x_N , since these

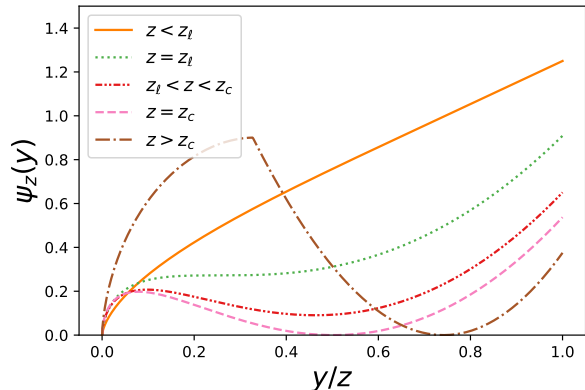


FIG. 4. The rate function $\psi_z(y)$, defined in Eq. (83), as a function of y/z , for different values of the z . For $z < z_\ell$, $\psi_z(y)$ has no minimum for $y > 0$. At $z = z_\ell$ a minimum appears at $y^* > 0$ with $\psi_z(y^*) > 0$. Increasing z further, the value of $\psi_z(y^*)$ decreases until for $z = z_c$ one finds that $\psi_z(y^*) = 0$. For $z > z_c$, one still has that $\psi_z(y^*) = 0$. Note that in this figure we plot $\psi_z(y)$ as a function of y/z so that curves corresponding to different values of z have the same range of values, since $0 < y < z$.

variables are i.i.d. Thus, given an RTP trajectory with total displacement X and choosing at random one of the N runs, $p(x|X)$ describes the distribution of the displacement x associated to that run. For simplicity we limit our discussion to the case $X > 0$: all arguments hold identically for $X < 0$, since $P(X, N)$ is symmetric around the origin.

The marginal probability $p(x|X)$, obtained from numerical simulations, is shown in Fig. 3 as a function of x for two different values of $z = X/N^{3/4}$. For $z < z_c$, we observe that $p(x|X)$ decays monotonically as a function of x . This observation is in agreement with the fact that in the fluid phase we expect each run to provide an order-one contribution to the total displacement. Upon crossing the critical point $z = z_c$, an additional bump appears in the tail of $p(x|X)$, signalling the presence of a condensate. The position of the bump scales with N as $N^{3/4}$ and it has Gaussian fluctuations of order \sqrt{N} .

It turns out that for $x \sim O(1)$ the PDF $p(x|X)$ is given to leading order by

$$p(x|X) \simeq \mathcal{P}(x) \quad (20)$$

where $\mathcal{P}(x)$ is given in Eq. (7). In other words, when $x \sim O(1)$, the marginal distribution $p(x|X)$ is simply given by the unconstrained PDF $\mathcal{P}(x)$. Note that this is valid for any $z > 0$, i.e., both in the fluid and the condensed phases. Indeed, in Fig. 3 we observe that the two numerical lines, obtained for $z < z_c$ and $z > z_c$, collapse into the same curve when $x \sim O(1)$.

Thus, in order to distinguish between fluid and condensed phase one has to study the tail behavior of $p(x|X)$. In particular, in the region where $x \sim O(N^{3/4})$ we find

that

$$p(x|X) \sim \exp \left[-\sqrt{N} \psi_z \left(\frac{x}{N^{3/4}} \right) \right], \quad (21)$$

where $z = X/N^{3/4}$,

$$\psi_z(y) = \frac{3}{2}y^{2/3} + F(z-y) - F(z), \quad (22)$$

and $F(z)$ is the rate function defined in Eq. (18). Thus, the probability of the rare fluctuations where $x \sim N^{3/4}$ is described by the rate function $\psi_z(y)$ (shown in Fig. 4), where $y = x/N^{3/4}$.

For $z < z_c$, the function $\psi_z(y)$ is always positive and thus the probability of configurations with $x \sim N^{3/4}$ decays as $e^{-c\sqrt{N}}$, where $c > 0$ is some positive constant. This can be observed in Fig. 3, where the empirical PDF $p(x|X)$ vanishes in the region $x \sim O(N^{3/4})$ for $z < z_c$. Conversely, for $z > z_c$ we find that there is a unique point $y^* > 0$ at which $\psi_z(y^*) = 0$ [the precise expression of y^* as a function of z is given in Eq. (H11)]. This zero of the rate function corresponds to the isolated bump in the tail of $p(x|X)$ at $x = y^*N^{3/4}$, as shown in Fig. 3.

Indeed, by expanding $p(x|X)$ in the vicinity of $x = y^*N^{3/4}$, we obtain

$$p(x|X) \simeq p_{\text{cond}}(x - y^*N^{3/4}, N), \quad (23)$$

where

$$p_{\text{cond}}(y, N) = \sqrt{\frac{\psi_z''(y^*)}{2\pi}} \frac{1}{N^{5/4}} \exp \left[-\frac{\psi_z''(y^*)y^2}{2N} \right], \quad (24)$$

and $\psi_z''(y)$ is the second derivative of $\psi_z(y)$ with respect to y . Thus, above the transition a bump appears in the tail of the marginal distribution at $x \simeq y^*N^{3/4}$, corresponding to a condensate with Gaussian fluctuations of order \sqrt{N} (see Fig. 3). Additionally, we show that

$$\int_{-\infty}^{\infty} dy p_{\text{cond}}(y, N) = \frac{1}{N}, \quad (25)$$

in agreement with the fact that any of the i.i.d. variables x_1, \dots, x_N can become the condensate. In other words, in the condensed phase, $N - 1$ displacements give an order-one contribution to the final position X , while a single displacement contributes to a finite fraction of X .

3. Order parameter: the participation ratio

Finally, we identify an order parameter for this first-order transition: the *participation ratio* $Y_2(z)$, defined as

$$Y_2(z) = \left\langle \frac{\sum_{i=1}^N x_i^2}{\left(\sum_{i=1}^N x_i \right)^2} \right\rangle_z, \quad (26)$$

where $\langle \dots \rangle_z$ denotes the statistical average of the distribution of the displacements $x_1 \dots x_N$, conditioned

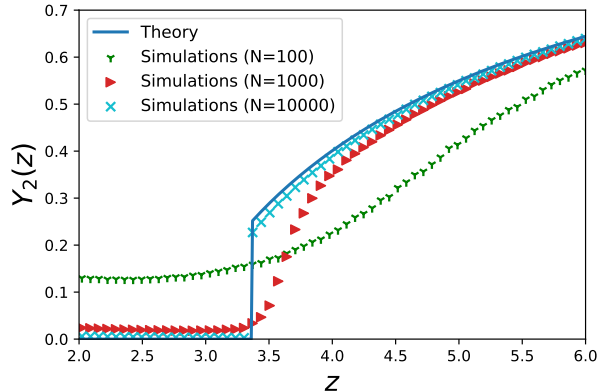


FIG. 5. The participation ratio $Y_2(z)$ as a function of the rescaled variable $z = X/N^{3/4}$. The continuous blue line represents the theoretical result in Eq. (27), while the symbols mark the results of numerical simulations, for different values of N . The participation ratio vanishes for $z < z_c = 2^{7/4}$, while it is positive for $z > z_c$. At the critical value $z = z_c$, $Y_2(z)$ has a jump discontinuity.

on the event $X = zN^{3/4}$. For $z < z_c$, the variables x_1, \dots, x_N contribute to the total displacement X by roughly the same amount of order one. Thus, the numerator in Eq. (26) scales as $O(N)$ while the denominator is equal to $X^2 \sim O(N^{3/2})$ and hence $Y_2(z) \sim O(1/\sqrt{N})$. On the other hand, in the condensed phase $z > z_c$ one single variable absorbs a finite fraction of X , while the other $N - 1$ variables remain of order one. Hence, both the denominator and the numerator in Eq. (26) scale as $O(N^{3/2})$ and we then expect $Y_2(z) \sim O(1)$. Indeed, we show that, in the large- N limit,

$$Y_2(z) = \begin{cases} 0 & \text{for } z < z_c, \\ [y^*(z)/z]^2 & \text{for } z > z_c, \end{cases} \quad (27)$$

where $y^*(z)$ is given in Eq. (H11). The expression for $Y_2(z)$ in Eq. (27) is shown in Fig. 5 and is in good agreement with numerical simulations. The participation ratio $Y_2(z)$ is the natural order parameter of the system. Indeed, $Y_2(z)$ is zero below the transition while it becomes non-zero for $z > z_c$. Notably, $Y_2(z)$ has a jump discontinuity at the critical value $z = z_c$, implying a first-order transition.

We show that the $Y_2(z)$ is related to the condensate fraction m_c , i.e., the fraction of the total displacement X which is carried by the condensate, by the simple relation

$$Y_2(z) = m_c^2. \quad (28)$$

We also compute the asymptotic behavior of $Y_2(z)$ in the region $z > z_c$, showing that

$$Y_2(z) \simeq \begin{cases} 1/4 + 2^{-7/4}(z - z_c) & \text{for } z \rightarrow z_c^+, \\ 1 - 4z^{-4/3} & \text{for } z \rightarrow \infty. \end{cases} \quad (29)$$

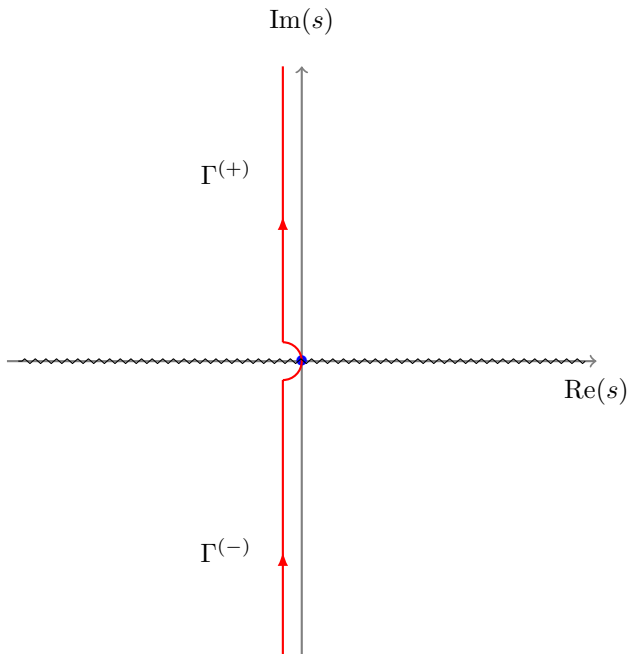


FIG. 6. Analytic properties in the complex- s plane of the function $\mathcal{L}(s)$, given in Eq. (34). The function $\mathcal{L}(s)$ is characterized by two branch cuts (black wiggled lines), which correspond to the intervals $] -\infty, 0[$ and $]0, \infty[$ in the real axis. The full red line represents the contour Γ that we choose to perform the integral in Eq. (33) (in the case $X > 0$).

We observe that, above the transition, a condensate forms and the participation ratio jumps to the finite value $1/4$, corresponding to $m_c = 1/2$, i.e., to a configuration where the condensate absorbs half of the total displacement X . Increasing z further, the participation ratio $Y_2(z)$ increases and it goes to 1 as $z \rightarrow \infty$. Note that a participation ratio equal to 1 corresponds to a configuration where the whole displacement X is absorbed by a single jump.

III. POSITION DISTRIBUTION

In this Section, we investigate the PDF $P(X, N)$ of the position X of the RTP after N running phases. By using the integral representation of the delta function

$$\delta(X) = \frac{1}{2\pi i} \int_{\Gamma} e^{-sX} ds, \quad (30)$$

where Γ is the imaginary-axis Bromwich contour in the complex s plane (see Fig. 6), one can decouple the integrals over the variables x_i in Eq. (12) and rewrite $P(X, N)$ as

$$P(X, N) = \frac{1}{2\pi i} \int_{\Gamma} ds e^{sX} [\mathcal{L}(s)]^N. \quad (31)$$

where

$$\mathcal{L}(s) = \int_{-\infty}^{\infty} dx e^{-sx} \mathcal{P}(x). \quad (32)$$

The expression in Eq. (31) can be then rewritten as

$$P(X, N) = \frac{1}{2\pi i} \int_{\Gamma} ds e^{sX+N \log[\mathcal{L}(s)]}. \quad (33)$$

The function $\mathcal{L}(s)$ can be explicitly computed by substituting the expression for $\mathcal{P}(x)$, given in Eq. (7), into Eq. (32), yielding

$$\mathcal{L}(s) = \sqrt{\pi} \frac{e^{-1/(2s^2)}}{\sqrt{-2s^2}} \operatorname{erfc} \left[\frac{1}{\sqrt{-2s^2}} \right]. \quad (34)$$

From a direct inspection of Eq. (34), one finds that the contour integral in Eq. (33) cannot be computed directly using a saddle point approximation. Indeed, looking at the analytic structure of the function $\mathcal{L}(s)$ in the complex plane in Fig. 6, we observe that $\mathcal{L}(s)$ is non-analytic on the full real line in the complex- s plane, except at $s = 0$ where it has a removable discontinuity with $\mathcal{L}(0) = 1$. In particular, the function $\mathcal{L}(s)$ is characterized by two branch cuts (the black wiggled lines in Fig. 6) in the intervals $] -\infty, 0[$ and $]0, \infty[$ in the real- s axis. Our main results for $P(X, N)$ are obtained by analyzing the contour integral in Eq. (33) in the large- N limit.

1. Typical regime

Let us first consider the typical regime where $X = z\sqrt{N}$, where the rescaled variable z can be positive or negative. To investigate this regime we can choose the contour of integration Γ to lie on the imaginary axis in the complex s plane. Performing the change of variable $s \rightarrow s/\sqrt{N}$ in Eq. (33), we obtain

$$P(X = z\sqrt{N}, N) = \frac{1}{2\pi i} \frac{1}{\sqrt{N}} \int_{\Gamma} ds e^{sz+N \log[\mathcal{L}(s/\sqrt{N})]}. \quad (35)$$

Expanding the expression of $\mathcal{L}(s)$, given in Eq. (34), for small $|s|$ with $\operatorname{Re}(s) = 0$, we find

$$\mathcal{L}(s) = 1 + s^2 + o(s). \quad (36)$$

Using this expansion in Eq. (35), we find that for large N

$$P(X = z\sqrt{N}, N) \simeq \frac{1}{2\pi i} \frac{1}{\sqrt{N}} \int_{\Gamma} ds e^{sz+s^2}. \quad (37)$$

Performing the Gaussian integral, we finally get for $N \gg 1$ and $|X| \sim \sqrt{N}$

$$P(X, N) \simeq \frac{1}{2\sqrt{\pi N}} \exp(-X^2/4N), \quad (38)$$

as given in the first line of Eq. (17). Note that this result in Eq. (38) is a simple consequence of the CLT.

2. Extreme large deviations

We now consider the regime of extreme large deviations, where X scales linearly with N . In the following, we will focus on the case $X > 0$. The complementary case $X < 0$ can be obtained by the symmetry $P(X, N) = P(-X, N)$.

To extract the atypical behavior of the PDF $P(X, N)$ in this regime from the integral representation in Eq. (33), it is useful to deform the contour Γ , as shown in Fig. 6. To be precise, we choose the contour to run parallel to the imaginary axis with $\text{Re}(s) < 0$. Note that the contour needs to be deformed to pass through the origin, due to the presence of the two branch cuts (see Fig. 6).

It is useful to define the variable $z = X/N > 0$. Performing the change of variable $s \rightarrow s/N$ in Eq. (33), we find

$$P(X = zN, N) = \frac{1}{2\pi i} \frac{1}{N} \int_{\Gamma} ds e^{sz + N \log[\mathcal{L}(s/N)]}. \quad (39)$$

We now need to expand $\mathcal{L}(s)$ for small $|s|$. We find that, when $\text{Im}(s) < 0$ and $\text{Re}(s) < 0$,

$$\mathcal{L}(s) \simeq 1 + s^2 + o(s^2). \quad (40)$$

On the other hand, when $\text{Im}(s) > 0$ and $\text{Re}(s) < 0$, we obtain

$$\mathcal{L}(s) \simeq 1 + s^2 + \frac{\sqrt{2\pi}}{\sqrt{-s^2}} e^{-1/(2s^2)} + o(s^2). \quad (41)$$

When $\text{Im}(s) > 0$, one has an additional non-analytic term in the expansion of $\mathcal{L}(s)$. Thus, it is useful to write the contour Γ as the union of the contours Γ^+ , in the positive imaginary semiplane, and Γ^- , in the negative imaginary semiplane. Plugging the expansions of $\mathcal{L}(s)$, given in Eqs. (40) and (41), into Eq. (39), we find

$$P(X = zN, N) \simeq \frac{1}{2\pi i} \frac{1}{N} \int_{\Gamma^-} ds e^{sz + s^2/N} \quad (42)$$

$$+ \frac{1}{2\pi i} \frac{1}{N} \int_{\Gamma^+} ds \exp \left[sz + \frac{s^2}{N} + N^2 \frac{\sqrt{2\pi}}{\sqrt{-s^2}} e^{-N^2/(2s^2)} \right].$$

Expanding for large N , we obtain

$$P(X = zN, N) \simeq \frac{1}{2\pi i} \frac{1}{N} \int_{\Gamma^-} ds e^{sz} \left(1 + \frac{s^2}{N} \right) \quad (43)$$

$$+ \frac{1}{2\pi i} \frac{1}{N} \int_{\Gamma^+} ds e^{sz} \left[1 + \frac{s^2}{N} + N^2 \frac{\sqrt{2\pi}}{\sqrt{-s^2}} e^{-N^2/(2s^2)} \right].$$

Regrouping the different terms we obtain

$$P(X = zN, N) \simeq \frac{1}{2\pi i} \frac{1}{N} \int_{\Gamma} ds e^{sz} \left(1 + \frac{s^2}{N} \right) \quad (44)$$

$$+ \frac{N}{\sqrt{2\pi i}} \int_{\Gamma^+} ds \exp [sz - N^2/(2s^2)] \frac{1}{\sqrt{-s^2}}.$$

It is possible to show that the term

$$\frac{1}{2\pi i} \frac{1}{N} \int_{\Gamma} ds e^{sz} \left(1 + \frac{s^2}{N} \right) \quad (45)$$

vanishes for any $z \neq 0$. Thus, we are left with the integral over the contour Γ^+ . To perform this integral, we rotate the contour anticlockwise by an angle of $\pi/2$ and we obtain, using the parametrization $s = ik$

$$P(X = zN, N) \simeq \frac{N}{\sqrt{2\pi}} \int_{-\infty}^0 \frac{dk}{k} \exp [ikz + N^2/(2k^2)]. \quad (46)$$

This integral can be computed exactly and we obtain in the regime where $X \sim N$

$$P(X, N) \simeq N \frac{1}{2\sqrt{2\pi}} G_{0,3}^{3,0} \left(\frac{X^2}{8} \left| \begin{array}{c} 0 \ 0 \ 0 \\ 0 \ 0 \ 1/2 \end{array} \right. \right), \quad (47)$$

where $G_{0,3}^{3,0}(x|\dots)$ is the Meijer G-function. Comparing this expression to the one for the marginal PDF $\mathcal{P}(x)$ of the single displacements [see Eq. (7)], we find that

$$P(X, N) \simeq N \mathcal{P}(X). \quad (48)$$

Finally, using the large- x expansion of $\mathcal{P}(x)$, given in Eq. (10), we obtain

$$P(X, N) \simeq N \frac{1}{\sqrt{3}|X|^{1/3}} e^{-\frac{3}{2}|X|^{2/3}}, \quad (49)$$

as we anticipated in Eq. (17).

The result in Eq. (48) can be interpreted as follows. In the extreme large deviation regime, the final position X is dominated by a single large displacement, which has probability weight $\mathcal{P}(X)$. Since this atypical displacement can be any of the N variables x_1, \dots, x_N , the factor N is also present.

3. Anomalous large deviations: matching regime

Finally, let us consider the intermediate regime where $X \sim N^{3/4}$, which interpolates between the typical regime and the extreme large-deviation regime. As discussed in Sec. II, this unusual scale $N^{3/4}$ can be obtained by matching the exponent X^2/N of the expression of $P(X, N)$ in the typical regime and the exponent $X^{2/3}$ of the extreme large-deviation regime [see the third line in Eq. (17)].

We will limit our discussion to the case $X > 0$. We consider again the contour Γ shown in Fig. 6. We define the variable $z = X/N^{3/4} > 0$, so that what we have to compute is:

$$P(X = zN^{3/4}, N) = \frac{1}{2\pi i} \int_{\Gamma} ds e^{szN^{3/4} + N \log[\mathcal{L}(s)]}. \quad (50)$$

By expanding $\log[\mathcal{L}(s)]$ around the origin, using the expressions in Eqs. (40) and (41), we get

$$P(X = zN^{3/4}, N) \simeq \frac{1}{2\pi i} \int_{\Gamma^-} ds e^{szN^{3/4} + Ns^2} + \frac{1}{2\pi i} \int_{\Gamma^+} ds e^{szN^{3/4} + Ns^2 + N\sqrt{2\pi}e^{-1/(2s^2)}/\sqrt{-s^2}}. \quad (51)$$

We then expand

$$\exp\left[N\sqrt{2\pi} \frac{e^{-1/(2s^2)}}{\sqrt{-s^2}}\right] \simeq 1 + N\sqrt{2\pi} \frac{e^{-1/(2s^2)}}{\sqrt{-s^2}}, \quad (52)$$

so that in we can rewrite $P(X, N)$ as the sum of a Gaussian term and an anomalous term

$$P(X, N) \simeq P_G(X, N) + P_A(X, N). \quad (53)$$

Where the Gaussian term is given by

$$P_G(X, N) = \frac{1}{2\pi i} \int_{-i\infty}^{i\infty} ds e^{szN^{3/4} + Ns^2} \quad (54)$$

and the anomalous term reads

$$P_A(X, N) = \frac{N}{i} \int_{\Gamma^+} ds \frac{1}{\sqrt{-s^2}} e^{szN^{3/4} + Ns^2 - 1/(2s^2)}. \quad (55)$$

Performing the Gaussian integral in Eq. (54), we find

$$P_G(X, N) = \frac{1}{2\sqrt{\pi N}} e^{-\sqrt{N}z^2/4}. \quad (56)$$

In order to evaluate the integral in Eq. (55) we first perform the change of variable $s \rightarrow s/N^{1/4}$, yielding

$$P_A(X, N) = \frac{N}{i} \int_{\Gamma^+} ds \frac{1}{\sqrt{-s^2}} e^{\sqrt{N}G_z(s)}, \quad (57)$$

where

$$G_z(s) = zs + s^2 - \frac{1}{2s^2}. \quad (58)$$

It turns out that the integral in Eq. (57) can be computed by means of saddle-point approximation only for $z > z_\ell = 4(2/3)^{3/4}$ (see Appendix C). Indeed, the saddle point equation

$$G'_z(s) = z + 2s + \frac{1}{s^3} = 0 \quad (59)$$

has real solutions in s only for $z > z_\ell$. Thus, for $z > z_\ell$ it is possible compute the integral in Eq. (57) by saddle point method and we obtain

$$P_A(X = zN^{3/4}, N) \sim e^{-\sqrt{N}\chi(z)}, \quad (60)$$

where the function $\chi(z)$ is computed exactly in Appendix C for $z > z_\ell$ and is given in Eq. (C10). Note that for

$z < z_\ell$ the integral in Eq. (57), even if hard to evaluate, is still well defined.

Plugging the expressions for $P_A(X, N)$ and $P_G(X, N)$, given in Eqs. (56) and (60), into Eq. (53), we find that

$$P(X = zN^{3/4}, N) \sim e^{-\sqrt{N}z^2/4} + e^{-\sqrt{N}\chi(z)}. \quad (61)$$

From this expression it is clear that for large N the two terms will compete, since the two exponents both scale as \sqrt{N} . In particular, for large N we find that

$$P(X = zN^{3/4}, N) \sim e^{-\sqrt{N}F(z)}, \quad (62)$$

where

$$F(z) = \min\left[\frac{z^2}{4}, \chi(z)\right], \quad (63)$$

where we know the expression of $\chi(z)$ only for $z > z_\ell$. Luckily, it turns out that $\chi(z) < z^2/4$ only for $z > z_c = 2^{7/4}$ and that $z_c > z_\ell$ (see Appendix E). Thus, we know the exact expression of $\chi(z)$ in the relevant region $z > z_c$ and we obtain

$$F(z) = \begin{cases} z^2/4 & \text{for } z < z_c, \\ \chi(z) & \text{for } z > z_c. \end{cases} \quad (64)$$

This rate function $F(z)$ is shown in Fig. 2 and is in good agreement with numerical simulations. From the first line in Eq. (64) it is clear that the probability $P(X, N)$ remains Gaussian outside of the typical regime and up to $X = z_c N^{3/4}$. Moreover, it is easy to check that $F'(z)$, i.e., the first derivative of the rate function, is discontinuous at $z = z_c$, corresponding to a first-order dynamical phase transition.

The expression in Eq. (61) clarifies the mechanism of the transition, which resembles a first-order phase transitions of classical thermodynamics. Indeed, the transition is the result of the competition between two phases: the fluid phase, whose probability is described by the Gaussian weight, and the condensed phase, associated with the anomalous weight. In particular, to each phase corresponds a rate function ($z^2/4$ for the fluid phase and $\chi(z)$ for the condensed phase), which plays the role of the free energy for out-of-equilibrium systems. At a given value of the control parameter z , the system will be in the phase with lower rate function. Thus, the critical point z_c is by definition the value for which the two rate functions are equal.

It is also possible to compute the asymptotics of $\chi(z)$ at the limits of its domain $[z_\ell, \infty[$ (see Appendix D). For $z \rightarrow z_\ell$ one obtains

$$\chi(z) = \sqrt{6} + o(1), \quad (65)$$

while for $z \rightarrow \infty$

$$\chi(z) = \frac{3}{2}z^{2/3} - z^{-2/3} + o(z^{-2/3}). \quad (66)$$

Using the expansion in Eq. (66) we find that, starting from the intermediate regime $X = zN^{3/4}$ and taking the limit $z \rightarrow \infty$, one get, to leading order,

$$P(X = zN^{3/4}, N) \sim e^{-\sqrt{N}(3/2)z^{2/3}}. \quad (67)$$

Finally, using $z = XN^{-3/4}$, we obtain

$$P(X, N) \sim e^{-(3/2)X^{3/2}}, \quad (68)$$

smoothly matching with the the expression of $P(X, N)$ in the extreme large deviation regime, where $X \sim N$ [see Eq. (17)].

IV. MARGINAL PROBABILITY DENSITY AND THE PARTICIPATION RATIO

In this section we consider the marginal distribution $p(x|X)$ of a single displacement x , conditioned on the value of the final position X . Note that x could be any of the i.i.d. displacements x_1, \dots, x_N , for example we can choose $x = x_1$. We focus on the intermediate regime $X = zN^{3/4}$ and $X > 0$. In the subcritical fluid phase $z < z_c$ we expect this distribution to be peaked around order-one values of x , since the different displacements x_1, \dots, x_N contribute to the final position by roughly the same amount. On the other hand, in the condensed phase $z > z_c$, we expect that one single displacement, which we will refer to as the *condensate*, contributes extensively to the final position X . We denote by m_c the fraction of the total displacement X which is in the condensate. For $z > z_c$, we expect that a bump, corresponding to the condensate, develops in the tail of the marginal distribution $p(x|X)$. Since the condensate could be any of the N displacements x_1, \dots, x_N , we expect the area under this bump to be $1/N$.

Our starting point is the joint probability of the displacements $\{x_i\} = x_1, \dots, x_N$ and of the final position $X = \sum_{i=1}^N x_i$, which is given by

$$p(\{x_i\}, X) = \prod_{i=1}^N \mathcal{P}(x_i) \delta\left(X - \sum_{i=1}^N x_i\right), \quad (69)$$

where $\mathcal{P}(x)$ is the unconstrained marginal probability, given in Eq. (7). From this expression, integrating over x_2, \dots, x_N , we obtain the PDF of x_1 and X

$$p(x_1, X) = \mathcal{P}(x_1) \int_{-\infty}^{\infty} dx_2 \dots \int_{-\infty}^{\infty} dx_N \left[\prod_{i=2}^N \mathcal{P}(x_i) \right] \times \delta\left(X - x_1 - \sum_{i=2}^N x_i\right). \quad (70)$$

Note that in principle one could choose, instead of x_1 , any of the variables x_1, \dots, x_N . Thus, from now on we will use the notation $x = x_1$. We notice that the term

$$\int_{-\infty}^{\infty} dx_2 \dots \int_{-\infty}^{\infty} dx_N \left[\prod_{i=2}^N \mathcal{P}(x_i) \right] \delta\left(X - x - \sum_{i=2}^N x_i\right), \quad (71)$$

is exactly equal to $P(X - x, N - 1)$, defined in Eq. (12). Thus, Eq. (70) becomes

$$p(x, X) = \mathcal{P}(x)P(X - x, N - 1). \quad (72)$$

Finally, since $p(x|X)$ is defined as the PDF of the single displacement x , conditioned on the final position X , we find

$$p(x|X) = \mathcal{P}(x) \frac{P(X - x, N - 1)}{P(X, N)}. \quad (73)$$

Note that since the N runs are identically distributed and the total displacement $X = \sum_i x_i$ is fixed, the first moment of $p(x|X)$ is given by

$$\int_{-\infty}^{\infty} dx x p(x|X) = \frac{X}{N}. \quad (74)$$

In particular, it is relevant to observe that even in the large-deviation regime, where $X \sim O(N^{3/4})$, the first moment of $p(x|X)$ vanishes as $N^{-1/4}$ for large N .

The main goal of this section is to analyze this marginal probability $p(x|X)$ in the intermediate large-deviation regime, where the dynamical phase transition occurs. In the previous section we have shown that, when $X = zN^{3/4}$, the distribution of X is given, in the large- N limit, by

$$P(X = zN^{3/4}, N) \sim e^{-\sqrt{N}F(z)}, \quad (75)$$

where $F(z)$ is given in Eq. (64). Plugging this expression into Eq. (73), for large N , we obtain

$$p(x|X) \sim \mathcal{P}(x)e^{-\sqrt{N}(F(z-y)-F(z))}, \quad (76)$$

where $y = x/N^{3/4}$ and $z = X/N^{3/4}$. Thus, when $x \ll N^{3/4}$ the rescaled variable y goes to zero for $N \rightarrow \infty$ and, expanding $F(z - y)$ for small y , we obtain

$$p(x|X) \simeq \mathcal{P}(x)e^{xF'(z)N^{-1/4}}. \quad (77)$$

Thus, for $x \ll N^{3/4}$, we find that to leading order the marginal PDF $p(x|X)$ is simply given by the unconstrained PDF $\mathcal{P}(x)$. The exponential correction factor in Eq. (77) skews the distribution $p(x|X)$ to the right (since $F'(z) > 0$ for $z > 0$). Thus, the value $F'(z)$ quantifies the asymmetry of $p(x|X)$.

Indeed, computing the average value of the PDF in Eq. (77) and expanding for large N , we find

$$\begin{aligned} & \int_{-\infty}^{\infty} dx x \mathcal{P}(x) e^{xF'(z)N^{-1/4}} \\ & \simeq \int_{-\infty}^{\infty} dx x \mathcal{P}(x) \left(1 + xF'(z)N^{-1/4}\right). \end{aligned} \quad (78)$$

Using the values of the first two moments of $\mathcal{P}(x)$, given in Eqs. (8) and (9), we obtain

$$\int_{-\infty}^{\infty} dx x \mathcal{P}(x) e^{xF'(z)N^{-1/4}} \simeq m_f \frac{X}{N}, \quad (79)$$

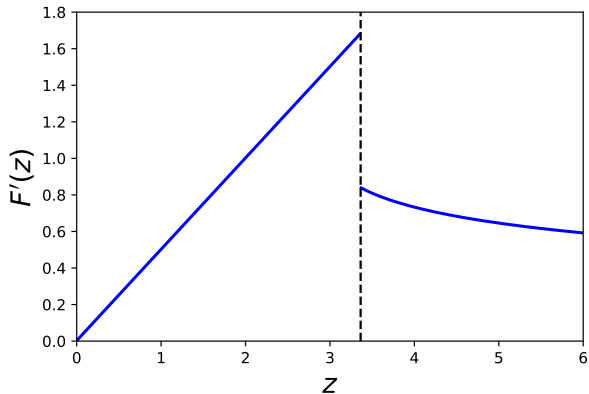


FIG. 7. First derivative of the rate function $F(z)$, given in Eq. (63), versus $z = X/N^{3/4}$.

where we have defined

$$m_f = \frac{2F'(z)}{z}. \quad (80)$$

We will call this quantity m_f *fluid fraction*, for reasons that will be clarified later in this section. Notably, using the expression of $F(z)$ in Eq. (63), we obtain $m_f = 1$ for $z < z_c$ and thus

$$\int_{-\infty}^{\infty} dx x \mathcal{P}(x) e^{xF'(z)N^{-1/4}} \simeq \frac{X}{N}, \quad (81)$$

in agreement with the strict conservation law in Eq. (74). However, at $z = z_c$ the function $F'(z)$ is discontinuous and it decreases with z for $z > z_c$ [see Fig. (7)]. Thus, for $z > z_c$, m_f becomes a decreasing function of z , meaning that increasing the value of the total displacement X the value of the typical single-run displacement x decreases.

This apparent contradiction is a consequence of the fact that the expression in Eq. (77) is only valid for $x \ll N^{3/4}$ and that the tail of the distribution $p(x|X)$ could in principle also contribute to the mean value. Thus, it is useful to consider the regime $x \sim N^{3/4}$ and to define the scaled variable $y = x/N^{3/4} \sim O(1)$. In this regime, plugging the large- x expansion of $\mathcal{P}(x)$, given in Eq. (10), into Eq. (76), we obtain

$$p(x|X) \sim e^{-\sqrt{N}\psi_z(x/N^{3/4})}, \quad (82)$$

where

$$\psi_z(y) = \frac{3}{2}y^{2/3} + F(z-y) - F(z), \quad (83)$$

and $F(z)$ is given in Eq. (64). We recall that $y = x/N^{3/4}$ and $z = X/N^{3/4}$. This rate function $\psi_z(y)$, parametrized by z , describes the probability of the large deviations where $x \sim O(N^{3/4})$. One can check that $\psi_z(y) \geq 0$ for any $z > 0$ and $y > 0$ (see Fig. 4).

It is instructive to investigate the behavior of $\psi_z(y)$ as a function of y , fixing z . For $z < z_\ell$, the function $\psi_z(y)$ is

monotonic in y (see Appendix H). On the other hand, for $z > z_\ell$ a local minimum appears at some value $y = y^* > 0$ [the precise value of y^* depends on z and is given in (H11)]. However, the value $\psi_z(y^*)$ corresponding to this minimum is initially strictly positive (see Fig. 4). Thus, configurations where $x = y^*N^{3/4}$ are still exponentially rare for large N and do not contribute to the average value of x .

Increasing z , this minimum $\psi_z(y^*)$ decreases, until, at the critical value $z = z_c$ it becomes zero. Thus, the configuration where $y = y^*$ becomes typical and a condensate develops at $x = x^*$, where $x^* = y^*N^{3/4}$. For $z > z_c$, there is always a unique value $y^* > 0$ at which $\psi_z(y^*) = 0$. This zero of the rate function $\psi_z(y)$ corresponds to the appearance of a bump in the tail of $p(x|X)$ and the value y^* increases as a function of z . Thus, for $z > z_c$ the fraction $m_c = x^*/X$ of the total displacement X that belongs to the condensate is given by

$$m_c = \frac{y^*N^{3/4}}{X} = \frac{y^*}{z}. \quad (84)$$

On the other hand, below the transition no condensate is present and thus $m_c = 0$. To summarize, we obtain

$$m_c = \begin{cases} 0 & \text{for } z < z_c, \\ y^*/z & \text{for } z > z_c, \end{cases} \quad (85)$$

where y^* is given in Eq. (H11). The condensate fraction m_c is shown in Fig. 8 as a function of z . In particular, in the region $z > z_c$ we obtain (see Appendix H)

$$m_c \simeq \begin{cases} 1/2 + (z - z_c)/2^{7/4} & \text{for } z \rightarrow z_c^+, \\ 1 - 2z^{-4/3} & \text{for } z \rightarrow \infty. \end{cases} \quad (86)$$

Thus, when crossing the transition line $z = z_c$, the fraction m_c jumps from zero to 1/2, signaling a first-order phase transition and a condensate, containing half of the total displacement X , appears. Increasing z further, the fraction m_c increases and it goes to one when $z \rightarrow \infty$. Thus, for $z \gg z_c$ almost the totality of the displacement X is in the condensate.

The behavior of $\psi_z(y)$ clarifies the mechanism of the dynamical transition, which turns out to be reminiscent of equilibrium first-order transitions. Indeed, the rate function $\psi_z(y)$ can be interpreted as the free energy of the system, while the variables y and z are the order and the control parameters, respectively. The global minimum of $\psi_z(y)$ corresponds to the most probable value of $y = x/N^{3/4}$. In the fluid phase, where the displacement x is of order one, the minimum is located at $y = 0$. On the other hand, in the condensed phase there is a single displacement with $x \sim O(N^{3/4})$, corresponding to $y > 0$. Indeed, above the critical point z_c , the rate function $\psi_z(y)$ has two degenerate global minima, at $y = 0$ and $y = y^* > 0$. This is in agreement with the fact

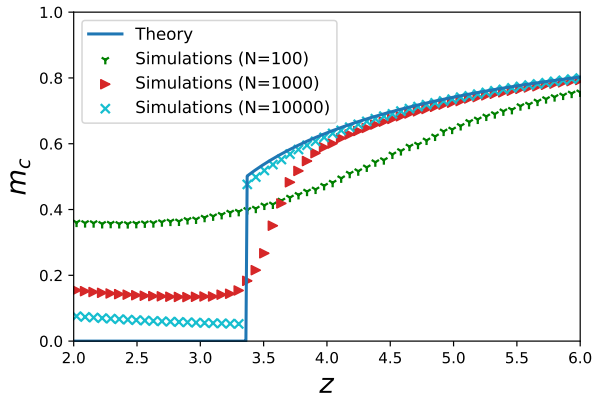


FIG. 8. The condensate fraction m_c as a function of $z = X/N^{3/4}$. The continuous blue line corresponds to the exact result in Eq. (85), while the symbols correspond to numerical simulations performed at different values of the number N of running phases

that $N - 1$ displacements are of order one (corresponding to $y = 0$) and one displacement is of order $N^{3/4}$ (corresponding to $y = y^*$). Finally, the fact that for $z_\ell < z < z_c$ a local minimum appears at $y = y^* > 0$ means that the condensed phase is metastable for this range of parameters.

Since the condensate is a single large run (see Appendix F), the fluid fraction m_f , defined in Eq. (80), can be interpreted as the fraction of the total displacement X associated to the other $N - 1$ running phases, whose displacements x_i are of order one. Indeed, using the expressions in Eqs. (80) and (85), it is possible to check that the condensate fraction m_c and the fluid fraction m_f sum to unity, i.e., that

$$m_c + m_f = 1. \quad (87)$$

For $z < z_c$, we have shown that $m_f = 1$ and $m_c = 0$. Just above the critical point $z = z_c$, the condensate fraction m_c jumps to the value $1/2$ and thus $m_f = 1/2$. Increasing z further, the value of m_c increases while m_f decreases. In the limit $z \rightarrow \infty$, we find that $m_c \rightarrow 1$ and $m_f \rightarrow 0$.

Once we have identified the location $y = y^*$ of the condensate, it is relevant to investigate its shape. To do this, we need to expand the expression in Eq. (82) around $y = y^*$. This yields, after few steps of algebra,

$$p(x|X) \simeq p_{\text{cond}}(x - y^* N^{3/4}, N) \quad (88)$$

where

$$p_{\text{cond}}(y, N) \sim \exp \left[-\frac{1}{2} \psi_z''(y^*) \frac{y^2}{N} \right]. \quad (89)$$

Here $\psi_z''(y)$ denotes the second derivative of $\psi_z(y)$, given in Eq. (83), with respect to y . To obtain the result in Eq. (88), we have used the fact that, above the transition, $\psi_z(y^*) = 0$ and $\psi_z'(y^*) = 0$. Overall, we have shown

that, above the transition, a condensate appears at $x = y^* N^{3/4}$, with a Gaussian shape and standard deviation which grows as \sqrt{N} .

It is also possible to compute the area under the bump, which corresponds to the probability that a given site becomes the condensate. To do this, one needs to compute carefully the prefactor in Eq. (88). We present the details of this computation in Appendix I, where we show that

$$p_{\text{cond}}(y, N) = \frac{1}{N^{3/2}} \sqrt{\frac{\psi_z''(y^*)}{\pi}} \exp \left[-\frac{1}{2} \psi_z''(y^*) \frac{y^2}{N} \right]. \quad (90)$$

From this expression, we obtain

$$\int_{-\infty}^{\infty} dy p_{\text{cond}}(y, N) = \frac{1}{N}, \quad (91)$$

meaning that above the transition the condensate is localized in just one of the N sites. Note that it is possible to show that in the thermodynamic limit there can be at most one condensate (see Appendix F).

Finally, we introduce another order parameter, the participation ratio, which is often considered in the literature of condensation transitions [34, 36]. This quantity $Y_2(z)$ is defined as

$$Y_2(z) = \left\langle \frac{\sum_{i=1}^N x_i^2}{\left(\sum_{i=1}^N x_i \right)^2} \right\rangle_z. \quad (92)$$

The notation $\langle \dots \rangle_z$ denotes the average over the distribution of the displacements x_1, \dots, x_N , conditioned on the value $X = zN^{3/4}$ of the total displacement. In the fluid phase, we expect the numerator in Eq. (92) to scale as $O(N)$, since the terms x_1, \dots, x_N are of order one. On the other hand, the denominator is equal to $X^2 \sim O(N^{3/2})$. Thus, for $z < z_c$ the participation ratio should vanish as $1/\sqrt{N}$. Conversely, in the condensed phase, a single variable x_i absorbs a finite fraction of the displacement X . Thus, both numerator and denominator are expected to scale as $N^{3/2}$ and $Y_2(z) \sim O(1)$ in the large N limit. For this reason, $Y_2(z)$ is a good order parameter for our system, where the corresponding control parameter is $z = X/N^{3/4}$.

Let us now compute the precise expression of $Y_2(z)$. First of all, using the fact that the variables x_i are independent and that the denominator in Eq. (92) is simply $X = zN^{3/4}$, we can rewrite the expression in Eq. (92) as

$$Y_2(z) = \frac{\langle x^2 \rangle_z}{z^2 \sqrt{N}}, \quad (93)$$

where

$$\langle x^2 \rangle_z = \int_{-\infty}^{\infty} dx x^2 p(x|X). \quad (94)$$

For $z < z_c$, using the expression of $p(x|X)$ in Eq. (77), it is easy to show that $\langle x^2 \rangle_z \sim O(1)$ and thus that $Y_2(z)$

vanishes as $1/\sqrt{N}$ in the large- N limit. Conversely, for $z > z_c$, we have shown that a bump appears in the tail of $p(x|X)$. It turns out that above the transition $\langle x^2 \rangle_z$ is dominated by the contribution coming from this condensate bump. Indeed, using the expression of $p(x|X)$ in the vicinity of the bump, given in Eq. (90), we obtain, to leading order,

$$\langle x^2 \rangle_z \simeq y^{*2} \sqrt{N}, \quad (95)$$

where y^* is given in Eq. (H11). Pugging this expression in Eq. (93), we obtain

$$Y_2(z) = \left(\frac{y^*}{z} \right)^2. \quad (96)$$

Recalling the expression of the condensate fraction m_c in Eq. (85), we find that the participation ratio and the condensate fraction are simply related by

$$Y_2(z) = m_c^2. \quad (97)$$

To summarize, we have shown that

$$Y_2(z) = \begin{cases} 0 & \text{for } z < z_c, \\ [y^*(z)/z]^2 & \text{for } z > z_c, \end{cases} \quad (98)$$

where $y^*(z)$ is given in Eq. (H11). This exact result is shown in Fig. (5) and is in good agreement with numerical simulations. Using the asymptic expressions of m_c in Eq. (86), we find

$$Y_2(z) \simeq \begin{cases} 1/4 + 2^{-7/4}(z - z_c) & \text{for } z \rightarrow z_c^+, \\ 1 - 4z^{-4/3} & \text{for } z \rightarrow \infty, \end{cases} \quad (99)$$

as given in Eq. (29).

V. CONCLUSIONS

In this paper, we have investigated the position distribution of a single RTP moving in one dimension. We have assumed that the velocity of the particle during each running phase is independently drawn from a Gaussian distribution. We have computed the PDF $P(X, N)$ of the position X of the particle after N running phases, showing that this PDF is characterized by three different regimes in the limit of large N . In the typical regime $X \sim O(\sqrt{N})$ and the distribution $P(X, N)$ has a Gaussian shape, as predicted by the CLT. On the other hand, in the extreme large deviation regime $X \sim O(N)$, the PDF $P(X, N)$ has a stretched exponential form, signaling that the full displacement X occurs in a single running phase. Finally, in the intermediate regime $X \sim O(N^{3/4})$, the PDF of X is described by the rate function $F(z)$, where $z = X/N^{3/4}$. Below the critical value z_c , $F(z)$ is

quadratic, meaning that $P(X, N)$ remains Gaussian up to $X = z_c N^{3/4}$, outside of the region predicted by the CLT. Interestingly, at the critical point z_c the rate function $F(z)$ is non-analytic and for $z > z_c$ it is not quadratic anymore. In particular, it turns out that the first derivative of $F(z)$ is discontinuous at $z = z_c$, corresponding to a first-order dynamical phase transition. Note that this type of condensation transition is not present in the standard RTP model, where the velocity of the particle is constant.

We have provided a detailed analysis of the mechanism of the phase transition. First of all, we have investigated the marginal probability $p(x|X)$ of a single-run displacement, conditioned on the total displacement X . We have shown that, above the transition, a bump appears in the tail of $p(x|X)$, suggesting that the system undergoes a condensation transition. In particular, we have shown that above the transition a single running phase contributes to a macroscopic fraction of X . In addition, we have identified a relevant order parameter associated to the phase transition: the participation ratio $Y_2(z)$. We have shown that $Y_2(z)$ is zero below the transition, it is non-zero for $z > z_c$. We have observed that this order parameter undergoes a jump $\Delta Y_2(z) = 1/4$ exactly at $z = z_c$, in agreement with the fact that the transition is first-order. Finally, we have performed extensive numerical simulations to confirm our theoretical results. In order to study numerically the probability of the rare events associated to the large-deviation regime, we have employed a constrained Markov chain Monte Carlo algorithm.

We have shown that the problem investigated in this paper can be mapped into the classical problem of finding the distribution of N i.i.d. random variables. Despite the apparent simplicity of the setup, we have observed that the PDF $P(X, N)$ is highly non-trivial in the large N limit and that a dynamical phase transition is observed above a critical value of X . As mentioned in the introduction, an alternative approach when studying the RTP model is to fix the total elapsed time T , instead of the number N of running phases. This corresponds to the fixed- T ensemble, which is usually harder to treat analytically. Even if we expect the late-time behavior to be similar for the fixed- N and fixed- T ensembles, for future works it would be relevant to investigate the large deviation regime of $P(X, T)$, i.e., the PDF of the RTP position X after time T . It would be interesting to compute the rate function associated to the large-deviation regime $X \sim O(T^{3/4})$ and to recover the first-order transition for this ensemble.

It is relevant to mention that if one considers a generic symmetric distribution $\mathcal{P}(x)$ with

$$\mathcal{P}(x) \sim e^{-a|x|^\beta}, \quad (100)$$

with $a > 0$ and $0 < \beta < 1$, the main results of this paper remain valid. Indeed, even if the scale at which the phase transition occurs is different [one can check

that $X_c \sim O(N^\alpha)$ with $\alpha = 1/(2 - \beta)$], the mechanism and the order of the transition remain the same.

Finally, let us also mention that the problem of computing the distribution of the sum of several i.i.d. variables with a stretched exponential PDF appears in many other situations, including the problem of localization in the discrete nonlinear Schrödinger equation [34, 35]. Another example can be found in the context of one-dimensional Brownian motion with resetting [57, 58]. Indeed, it is easy to show that the integral of the position of the Brownian particle between two resetting events will have a stretched-exponential distribution with $\beta = 1/2$, where β is the exponent defined in Eq. (100). For this reason, the integral of the position of the resetting Brownian motion can be written as the sum of several i.i.d. stretched-exponential variables and the system will display a first-order condensation transition at late times. Thus, we expect our results to be applicable to several problems besides the one considered in this paper.

ACKNOWLEDGMENTS

We thank P. Le Doussal, R. Livi and G. Schehr for useful discussions. G.G. acknowledges Financial support from ERC Grant No. ADG20110209, and from the Simons Foundation gran No. 454949.

Appendix A: Asymptotic tails of $\mathcal{P}(x)$

In this Appendix we derive the asymptotic tails of $\mathcal{P}(x)$ given in Eq. (6). Let us focus on the case $x > 0$ with $x \gg 1$. Performing the change of variable $\tau \rightarrow y = \tau/x^{2/3}$ in Eq. (6), we obtain

$$\mathcal{P}(x) = \frac{1}{\sqrt{2\pi}} \int_0^\infty dy \frac{1}{y} e^{-x^{2/3}[y+1/(2y^2)]}. \quad (\text{A1})$$

For large x , this integral can be performed by saddle-point approximation, which yields

$$\mathcal{P}(x) \simeq \frac{1}{\sqrt{3}x^{1/3}} e^{-(3/2)x^{2/3}}. \quad (\text{A2})$$

Repeating this argument in the case of $x < 0$ with $|x| \gg 1$, we obtain

$$\mathcal{P}(x) \simeq \frac{1}{\sqrt{3}|x|^{1/3}} e^{-(3/2)|x|^{2/3}}. \quad (\text{A3})$$

as given in Eq. (10).

Appendix B: Numerical simulations in the large-deviation regime

In this Appendix, we present the details of the numerical simulations that we have performed to confirm our

analytical results. In order to study the large-deviation regime we employ a constrained MCMC algorithm, similar to the ones used in Refs. [26, 29, 59, 60].

An RTP configuration with N steps is described by the N couples $\{(\tau_i, v_i)\} = \{(\tau_1, v_1), \dots, (\tau_N, v_N)\}$. The probability weight associated to each configuration is

$$P(\{(\tau_i, v_i)\}) = \prod_{i=1}^N p(\tau_i)W(v_i), \quad (\text{B1})$$

where $p(\tau)$ and $W(v)$ are given in Eqs. (2) and (3). The position X of the particle after N steps is given by

$$X = \sum_{i=1}^N \tau_i v_i. \quad (\text{B2})$$

We want to estimate numerically the PDF $P(X, N)$ of the position X , in the limit of large N . If one is just interested in the typical fluctuations corresponding to $X \sim O(\sqrt{N})$, it is enough to employ a direct sampling strategy, drawing for each sample N independent running times $\tau_1 \dots \tau_N$ from the PDF $p(\tau)$ and N velocities v_1, \dots, v_N from $W(v)$. If one considers 10^6 samples, this method allows to reach events that occur with probability of order 10^{-6} or higher. However, to sample the rare events corresponding to the large-deviation regime where $X \sim O(N^{3/4})$ one has to use a more sophisticated technique. Indeed, these events have probability smaller than 10^{-100} and direct sampling algorithms are not computationally feasible.

For this reason, we use a biased MCMC algorithm, which allows us to sample rare configurations which are characterized by an atypically large displacement X . First, we implement a MCMC dynamics in the space of configurations $\{(\tau_i, v_i)\}$, using the Metropolis-Hastings algorithm to guarantee that the RTP trajectories are sampled with the correct statistical weight. In particular, starting from any initial configuration, we choose the i -th running phase, where i is a uniformly distributed random integer between 1 and N , and we propose a move $(\tau_i, v_i) \rightarrow (\tau_i^{\text{new}}, v_i^{\text{new}})$, where

$$\tau_i^{\text{new}} = \tau_i + \delta\tau_i, \quad (\text{B3})$$

and

$$v_i^{\text{new}} = v_i + \delta v_i. \quad (\text{B4})$$

Here $\delta\tau_i$ and δv_i are uniform random numbers in the intervals $(-a, a)$ and $(-b, b)$, respectively, where a and b are parameters of the algorithm. The move is accepted with probability

$$p_{\text{acc}} = \min \left[1, \frac{p(\tau_{\text{new}}^i)W(v_{\text{new}}^i)}{p(\tau^i)W(v^i)} \right], \quad (\text{B5})$$

and rejected otherwise. Initially, we let the system evolve for 10^7 sweeps, i.e., $10^7 N$ moves, in order to let the MCMC thermalize and then we measure the position X

of the RTP every 10^2 sweeps, to avoid correlations. From these samples, we build a histogram that approximates the PDF $P(X, N)$. Up to this point, the MCMC algorithm is completely equivalent to the direct sampling strategy and it only allows to sample typical trajectories.

In order to investigate the large deviations of $P(X, N)$, we need to bias the MCMC dynamics towards large values of X . For the sake of simplicity we will focus on positive values of X , the case $X < 0$ can be treated analogously. We start by choosing some large value X^* . Since we want to investigate the regime where $X \sim O(N^{3/4})$, we will take $X^* \sim O(N^{3/4})$. We initialize the MCMC from some initial condition with $X > X^*$. Then, we evolve the system according to the MCMC dynamics described above, adding the hard constraint $X > X^*$. In other words, attempted updates corresponding to $X < X^*$ are always rejected.

The histogram that we obtain from this biased algorithm will approximate the PDF $P(X, N|X > X^*)$, i.e., the PDF of X conditioned on the event $X > X^*$. This quantity is then simply related to the PDF $P(X, N)$ by, for $X > X^*$,

$$P(X, N|X > X^*) = \frac{P(X, N)}{P(X > X^*)}. \quad (\text{B6})$$

Taking the natural logarithm of both sides, we obtain

$$\begin{aligned} \log [P(X, N|X > X^*)] \\ = \log [P(X, N)] - \log [P(X > X^*)]. \end{aligned} \quad (\text{B7})$$

Diving both sides by \sqrt{N} and recalling that in the large- N limit the rate function $F(z)$ is defined as

$$F\left(\frac{X}{N^{3/4}}\right) = -\frac{\log [P(X, N)]}{\sqrt{N}}, \quad (\text{B8})$$

we find

$$F\left(\frac{X}{N^{3/4}}\right) = -\frac{\log [P(X, N|X > X^*)]}{\sqrt{N}} + C_{X^*}. \quad (\text{B9})$$

In the equation above, we have defined the constant (with respect to X)

$$C_{X^*} = \frac{\log [P(X > X^*)]}{\sqrt{N}}. \quad (\text{B10})$$

Thus, in order to estimate numerically $F(z)$ we need to compute the value of C_{X^*} . This can be achieved by the following strategy. First, we perform an unbiased simulation, which will allow us to estimate $F(z)$ in a small interval around the origin. Then, we choose a value of X^* such that $z^* = X^*/N^{3/4}$ falls within the range of values for which $F(z)$ is known. The biased simulation will give us an estimate of $F(z)$ in a small region with $z > z^*$, up to the constant C_{X^*} . Since the two estimates of $F(z)$, the one obtained without the constraint and the one with the constraint, overlap for some values of z , one can compute the constant C_{X^*} by matching the two

curves. This allows us to know $F(z)$ in a slightly larger interval. Then, we continue by performing a new MCMC simulation with a larger value of X^* and so on until $F(z)$ is known in a large-enough interval. Note that to speed up the algorithm the procedure above can be parallelized by choosing a fine enough grid of values X^* in order to ensure the overlap between the different histograms. For instance, to obtain the numerical curves in Fig. 2 we have used 90 equispaced values of X^* .

Let us also mention that with the technique described above one can also obtain the marginal PDF $p(x|X)$ (see Fig. 3). From the MCMC dynamics one has access to the values of the single-run displacements x_1, \dots, x_N . Measuring a randomly chosen displacement at every step one can build an histogram which will approximate the PDF $p(x|X > X^*)$. However, it turns out that when X^* is large, the system will typically stay in a small region to the right of X^* . In other words, even if X is free to fluctuate during the simulation, it will typically remain close to X^* . Thus, one can approximate

$$p(x|X > X^*) \simeq p(x|X^*). \quad (\text{B11})$$

Alternatively, one can avoid this approximation by performing a MCMC dynamics at fixed X (e.g., by proposing moves that conserve the total displacement X). However, the convergence of the algorithm turns out to be slower in this case. With the same technique one can also estimate Y_2 and m_c as functions of z (see Figs. 5 and 8). The results of our numerical simulations are in good agreement with the theory.

Appendix C: Exact computation of the function $\chi(z)$

Our starting point is the integral in Eq. (57), which reads

$$\begin{aligned} P_A(X = zN^{3/4}, N) \\ = \frac{1}{\sqrt{2\pi i}} N \int_{\Gamma^+} ds \frac{1}{\sqrt{-s^2}} e^{\sqrt{N}G_z(s)}. \end{aligned} \quad (\text{C1})$$

where

$$G_z(s) = zs + s^2 - \frac{1}{2s^2}. \quad (\text{C2})$$

We recall that we are considering the case $z > 0$ and that the integral in Eq. (C1) is performed over the contour Γ^+ in the complex s plane, running in the negative real semiplane, parallel to the imaginary axis and with $\text{Im}(s) > 0$ and with $\text{Re}(s) \rightarrow 0^-$ (see Fig. 6).

Our goal is to perform this integral by saddle-point approximation. To do that, let us consider the saddle-point equation

$$G'_z(s) = z + 2s + \frac{1}{s^3} = 0, \quad (\text{C3})$$

where $G'_z(s)$ indicates the first derivative of $G_z(s)$ with respect to s . This function $G'_z(s)$ is shown in Fig. 9 as a

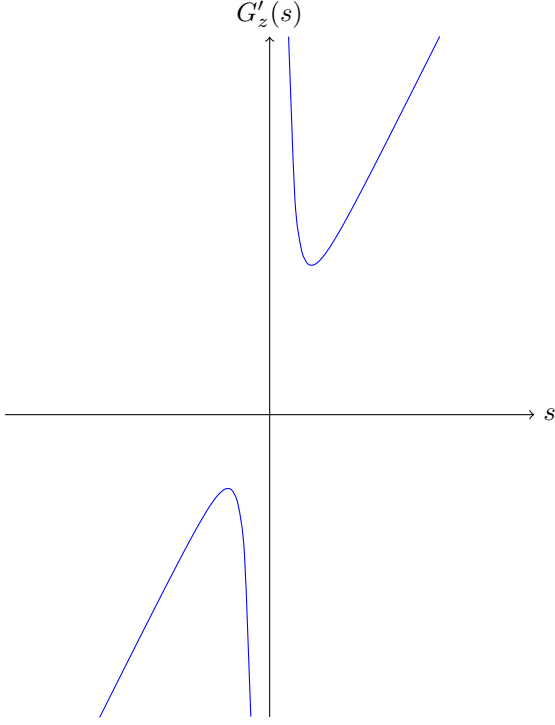


FIG. 9. Plot of $G'_z(s)$, given in Eq. (C3) as a function of s , for $z = 1$. For this value of z the saddle point condition in Eq. (C3) has no real solutions.

function of s for $z = 1$. It is clear from Fig. 9 that Eq. (C3) has no real solution for $z = 1$. However, increasing z amounts to a rigid upward vertical translation of the curve in Fig. 9. Thus, at a critical value of z , that we call z_ℓ , the $G'_z(s)$ curve will hit the negative s axis and the saddle point equation (C3) will have a single real solution $s^* < 0$. Increasing z further, Eq. (C3) will have two real solutions, which we denote by s_1 and s_2 , with $s_1 < s_2 < 0$. It is easy to check that s_1 corresponds to a minimum of $G_z(s)$, while s_2 corresponds to a maximum.

Thus, for $z > z_\ell$ the complex integral in Eq. (C1) can be computed as follows. First, we rotate the contour Γ^+ anticlockwise by an angle $\pi/2$, so that it now passes through the saddle points s_1 and s_2 . Then, since s_2 is a maximum, the integral will be dominated, for large N ,

by contributions close to s_2 and one obtains

$$P_A(X = zN^{3/4}, N) \simeq \frac{1}{-s_2 \sqrt{-G''_z(s_2)}} N^{3/4} e^{-\sqrt{N}\chi(z)},$$

where

$$\chi(z) = -G_z(s_2), \quad (\text{C4})$$

and

$$G''_{z_\ell}(s_2) = 2 - \frac{3}{s_2^4} < 0, \quad (\text{C5})$$

where $G''_z(s)$ denotes the second derivative of $G_z(s)$ with respect to s .

We now need to compute the limit value z_ℓ , which can be identified with the following argument. As explained above, at $z = z_\ell$, the saddle-point condition in Eq. (C3) will have exactly one real solution $s^* < 0$. Thus, s^* satisfies the condition

$$z_\ell + 2s^* + \frac{1}{s^{*3}} = 0. \quad (\text{C6})$$

Moreover, it is clear from Fig. 9 that at $z = z_\ell$ the point s^* corresponds to a maximum of the function $G'_z(s)$. Thus, one also has the condition

$$G''_{z_\ell}(s^*) = 2 - \frac{3}{s^{*4}} = 0. \quad (\text{C7})$$

Solving the two conditions in Eqs. (C6) and (C7), one finally finds that

$$s^* = -\left(\frac{3}{2}\right)^{1/4} \quad (\text{C8})$$

and

$$z_\ell = 4\left(\frac{2}{3}\right)^{3/4} = 2.95115\dots \quad (\text{C9})$$

Then, for $z > z_\ell$ the saddle point s_2 is defined as the largest real root of Eq. (C3) and can be computed by using Mathematica. Plugging this expression for s_2 into the definition of $\chi(z)$ in Eq. (C4), we find that

$$\begin{aligned} \chi(z) = & z^{2/3} \left(\frac{z^{4/3}}{8} + \frac{1}{8} \left(\frac{64(2/3)^{1/3}}{a(z)} + 4(2/3)^{2/3} a(z) z^{4/3} + z^{8/3} \right)^{1/2} - \frac{1}{2} \left(-\frac{4(2/3)^{1/3}}{a(z)} - \frac{a(z)z^{4/3}}{2 \cdot 2^{1/3} 3^{2/3}} + \frac{z^{8/3}}{8} \right. \right. \\ & \left. \left. + \frac{z^4}{8\sqrt{\frac{64(2/3)^{1/3}}{a(z)} + 4\left(\frac{2}{3}\right)^{2/3} a(z) z^{4/3} + z^{8/3}}} \right)^{1/2} \right)^{-2} + \frac{z^{2/3}}{2} \left(-\frac{z^{4/3}}{8} - \frac{1}{8} \sqrt{\frac{64(2/3)^{1/3}}{a(z)} + 4(2/3)^{2/3} a(z) z^{4/3} + z^{8/3}} \right. \\ & \left. + \frac{1}{2} \left(-\frac{4\left(\frac{2}{3}\right)^{1/3}}{a(z)} - \frac{a(z)z^{4/3}}{2 \cdot 2^{1/3} 3^{2/3}} + \frac{z^{8/3}}{8} + \frac{z^4}{8\sqrt{\frac{64(2/3)^{1/3}}{a(z)} + 4(2/3)^{2/3} a(z) z^{4/3} + z^{8/3}}} \right)^{1/2} \right), \quad (\text{C10}) \end{aligned}$$

where

$$a(z) = \left(9 + \sqrt{3} \sqrt{27 - \frac{2048}{z^2}} \right)^{1/3}. \quad (\text{C11})$$

Appendix D: Asymptotics of $\chi(z)$

In this section we want to compute the asymptotics of the function $\chi(z)$ at the edges of its domain $z_\ell < z < \infty$.

When $z \rightarrow z_\ell$ we already know that $s_2 \rightarrow s^*$. Thus, plugging the value of s^* , given in Eq. (C8), into the definition of $\chi(z)$, given in Eq. (C4), we find that when $z \rightarrow z_\ell$

$$\chi(z) \rightarrow \sqrt{6}, \quad (\text{D1})$$

as given in Eq. (19).

In order to investigate the limit $z \rightarrow \infty$, it is useful to define the variable

$$\phi = -z^{1/3} s. \quad (\text{D2})$$

Then the saddle point equation (C3) can be rewritten in terms of ϕ as

$$2z^{-4/3} \phi^4 - \phi^3 + 1 = 0. \quad (\text{D3})$$

Note that after the transformation in Eq. (D2), the relevant saddle point is the smallest positive root ϕ_2 of Eq. (D3). Using the expression of the function $G_z(s)$, given in Eq. (C2), and the definition of $\chi(z)$, given in Eq. (C4), we obtain

$$\chi(z) = z^{2/3} \left(\frac{1}{2} \phi_2 + \frac{1}{\phi_2^2} \right). \quad (\text{D4})$$

It turns out that Eq. (D3) is particularly useful to compute the large- z asymptotics. Indeed, for large z , Eq. (D3) can be solved perturbatively and one obtains

$$\phi_2 = 1 + \frac{2}{3} z^{-4/3} + o(z^{-4/3}). \quad (\text{D5})$$

Plugging this expansion into Eq. (D4) and expanding for large z , we obtain

$$\chi(z) = \frac{3}{2} z^{3/2} - z^{-2/3} + o(1), \quad (\text{D6})$$

as given in Eq. (19).

Appendix E: Computation of the critical point z_c

In the main text we have shown that the rate function for the intermediate matching regime is given by [see Eq. (63)]

$$F(z) = \min \left[\frac{z^2}{4}, \chi(z) \right], \quad (\text{E1})$$

where $\chi(z)$ is given in Eq. (C10). It is easy to check, for instance numerically, that $\chi(z) > z^2/4$ for $z > z_c$, where z_c is a constant of order one. Thus, one obtains

$$F(z) = \begin{cases} z^2/4 & \text{for } z < z_c, \\ \chi(z) & \text{for } z > z_c. \end{cases} \quad (\text{E2})$$

In this section, we want to compute exactly the critical point z_c , which is defined by the equation

$$\chi(z_c) = z_c^2/4. \quad (\text{E3})$$

Computing z_c starting from the explicit expression of $\chi(z)$ in Eq. (C10) appears to be rather challenging. However, using the representation of $\chi(z)$, given in Eq. (D4), in terms of the variable ϕ , defined in Eq. (D2), solving Eq. (E3) becomes simpler. First of all, from Eq. (D3), evaluated at the critical point $z = z_c$, we find that

$$z_c = \left(\frac{\phi_2^3 - 1}{2\phi_2^4} \right)^{-3/4}, \quad (\text{E4})$$

where we recall that ϕ_2 is the smallest positive root of Eq. (D3). Plugging the representation of $\chi(z)$ in terms of ϕ_2 , given in Eq. (D4), into Eq. (E3), we obtain

$$z_c^{2/3} \left(\frac{1}{2} \phi_2 + \frac{1}{\phi_2^2} \right) = z_c^2/4. \quad (\text{E5})$$

Finally, solving Eqs. (E4) and (E5), it is easy to show that

$$z_c = 2^{7/4} = 3.36359 \dots \quad (\text{E6})$$

Appendix F: The number of condensates

In this appendix, we show that configurations with two condensates are less likely with respect to those with a single condensate. We start by rewriting the expression in Eq. (12) as

$$P(X, N) = \int_{-\infty}^{\infty} dx_1 \mathcal{P}(x_1) \int_{-\infty}^{\infty} dx_2 \mathcal{P}(x_2) \quad (\text{F1}) \\ \times \prod_{i=3}^N \int_{-\infty}^{\infty} dx_i \mathcal{P}(x_i) \delta \left(X - x_1 - x_2 - \sum_{i=3}^N x_i \right),$$

where $\mathcal{P}(X)$ is the single-run PDF, given in Eq. (5). Using again Eq. (12), we can write Eq. (F2) as

$$P(X, N) = \int_{-\infty}^{\infty} dx_1 \mathcal{P}(x_1) \int_{-\infty}^{\infty} dx_2 \mathcal{P}(x_2) \\ \times P(X - x_1 - x_2, N - 2). \quad (\text{F2})$$

In the regime $X \sim O(N^{3/4})$ we use the large deviation form of $P(X, N)$, given in Eq. (17), and the large- x behavior of $\mathcal{P}(x)$, given in Eq. (10), and we obtain

$$e^{-\sqrt{N}F(X/N^{3/4})} \sim \int_{-\infty}^{\infty} dx_1 \int_{-\infty}^{\infty} dx_2 \quad (\text{F3}) \\ \times e^{-\sqrt{N}F[(X-x_1-x_2)/N^{3/4}] - (3/2)|x_1|^{2/3} - (3/2)|x_2|^{2/3}}.$$

Note that we are using the large- x asymptotics of $\mathcal{P}(x)$ because we are probing for configurations where x_1 and x_2 represent two condensates and hence are of order $O(N^{3/4})$. Using the scaled variables $z = X/N^{3/4}$, $y_1 = x_1/N^{3/4}$, and $y_2 = x_2/N^{3/4}$, we obtain the relation

$$e^{-\sqrt{N}F(z)} \sim \int_{-\infty}^{\infty} dy_1 \int_{-\infty}^{\infty} dy_2 \quad (\text{F4})$$

$$\times e^{-\sqrt{N}\{F[(z-y_1-y_2)/N^{3/4}] + (3/2)|y_1|^{2/3} + (3/2)|y_2|^{2/3}\}}.$$

The variables y_1 and y_2 represent the fraction of the total displacement contained in the two condensates. Thus, the presence of two condensate would correspond to both $y_1 > 0$ and $y_2 > 0$. Performing both integrals via saddle-point approximation, we find

$$F(z) \quad (\text{F5})$$

$$= \min_{0 \leq y_1 \leq z} \min_{0 \leq y_2 \leq z - y_1} \left[F(z - y_1 - y_2) + \frac{3}{2}y_1^{2/3} + \frac{3}{2}y_2^{2/3} \right].$$

Performing the change of variables $(y_1, y_2) \rightarrow (y_1, y = y_1 + y_2)$, we obtain

$$F(z) \quad (\text{F6})$$

$$= \min_{0 \leq y \leq z} \min_{0 \leq y_1 \leq y} \left[F(z - y) + \frac{3}{2}y_1^{2/3} + \frac{3}{2}(y - y_1)^{2/3} \right],$$

which can be rewritten as

$$F(z) \quad (\text{F7})$$

$$= \min_{0 \leq y \leq z} \left[F(z - y) + \min_{0 \leq y_1 \leq y} \left(\frac{3}{2}y_1^{2/3} + \frac{3}{2}(y - y_1)^{2/3} \right) \right].$$

It is easy to show that the minimum over y_1 is obtained for $y_1 = 0$ and $y_2 = y > 0$, or by symmetry for $y_2 = 0$ and $y_1 = y > 0$. Recalling that the presence of two condensates would require both $y_1 > 0$ and $y_2 > 0$, we have shown that configurations with two condensates cannot be observed in this model when $N \rightarrow \infty$.

Note that we have also verified that there can be only one condensate by showing that [see Eq. (25)]

$$\int_{-\infty}^{\infty} dy p_{\text{cond}}(y, N) = \frac{1}{N}, \quad (\text{F8})$$

i.e., that the area under the condensation bump is $1/N$. This is in agreement with the fact that only one of the N running phases can become the condensate.

Appendix G: Equivalence with the result of Ref. [53]

In Ref. [53] Brosset et al. derived by mathematical methods the rate function $F(z)$, defined in Eq. (1), showing that

$$F(z) = \min_{0 \leq y \leq z} \left[\frac{(z - y)^2}{4} + \frac{3}{2}y^{2/3} \right]. \quad (\text{G1})$$

At first sight, this result seems different from the one derived in this paper and given in Eq. (18). However,

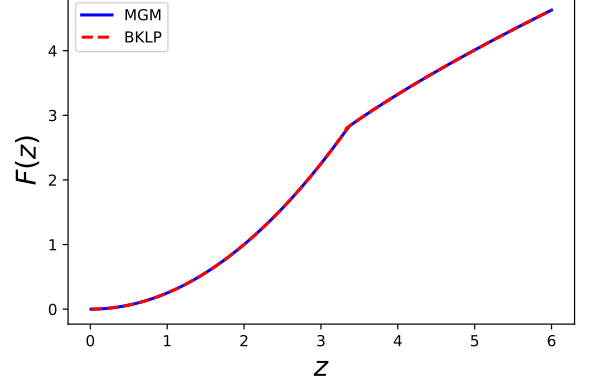


FIG. 10. Comparison between the rate function $F(z)$ computed by Brosset et al. (BKLP), given in Eq. (G1), and our result (MGM), given in Eq. (18).

performing the minimization numerically, we find that they are equivalent [see Fig. 10]. In this appendix we show analytically that the two expressions are equivalent.

Let us define

$$g_z(y) = \frac{(z - y)^2}{4} + \frac{3}{2}y^{2/3}, \quad (\text{G2})$$

so that we can write the expression in Eq. (G1) as

$$F(z) = \min_{0 \leq y \leq z} g_z(y) \quad (\text{G3})$$

Thus, we look for the solution y^* of the equation

$$g'_z(y^*) = \frac{y^* - z}{2} + y^{*-1/3} = 0. \quad (\text{G4})$$

Moreover, since y^* is a minimum, it also satisfies

$$g''_z(y^*) = -\frac{1}{3}y^{*-4/3} + \frac{1}{2} > 0. \quad (\text{G5})$$

Note that the minimum of $g_z(y)$ could be also reached at $y = 0$ or $y = z$.

One can show that y^* is related to the solution ϕ_2 of the saddle point equation (D3) by the relation

$$y^* = z\phi_2^{-3}. \quad (\text{G6})$$

Note that both y^* and ϕ_2 depend on z . Thus, from Appendix D, we know that Eq. (G4) will have no solution for $z < z_\ell$, implying that the minimum will be reached either at $y = 0$ or at $y = z$. It is easy to show that, for $z < z_\ell$, $g_z(0) < g_z(z)$ and therefore we obtain

$$F(z) = g_z(0) = \frac{z^2}{4}, \quad (\text{G7})$$

for $z < z_\ell$. In the region $z > z_\ell$ a solution y^* of Eq. (G4) that satisfy the condition (G5) exists. However, it is easy to check that just above z_ℓ the global minimum is still

reached at $y = 0$. Increasing z , the value of the minimum corresponding to y^* decreases until at some value $z = z_c$, the global minimum is reached at $y = y^*$. Thus, the critical point $z = z_c$ is defined as

$$g_{z_c}(0) = g_{z_c}(y^*), \quad (\text{G8})$$

where y^* is the solution of Eq. (G4) that satisfies the condition (G5). One can check that the point $y = z$ is never the global minimum.

Plugging the expression of $g_z(y)$, given in Eq. (G2), into Eq. (G8), we find that z_c satisfies

$$\frac{z_c^2}{4} = \frac{(z_c - y^*)^2}{4} + \frac{3}{2}y^{*2/3}. \quad (\text{G9})$$

Using Eq. (G6), we get

$$\frac{z_c^2}{4} = \frac{(z_c - z_c\phi_2^{-3})^2}{4} + \frac{3}{2}(z_c\phi_2^{-3})^{2/3}, \quad (\text{G10})$$

where we recall that ϕ_2 is the smallest positive solution of the saddle point equation (D3). Moreover, from Eq. (D3), we obtain

$$z^{4/3} = 2 \frac{\phi_2^4}{\phi_2^3 - 1}. \quad (\text{G11})$$

Eq. (G10) can be rewritten as

$$\frac{z_c^{4/3}}{4} [1 - (1 - \phi_2^{-3})^2] = \frac{3}{2}\phi_2^{-2}. \quad (\text{G12})$$

Plugging the expression for $z_c^{4/3}$ given in Eq. (G11) and solving for ϕ_2 yields

$$\phi_2 = 2^{1/3}, \quad (\text{G13})$$

for $z = z_c$. Using Eq. (G11), we obtain $z_c = 2^{7/4}$. Thus, for $z < z_c$ we have shown that

$$F(z) = \frac{z^2}{4}, \quad (\text{G14})$$

in agreement with our result in Eq. (18).

Finally, we need to show that for $z > z_c$ the two results in Eqs. (G1) and (18) coincide, i.e., that

$$\frac{(z - y^*)^2}{4} + \frac{3}{2}y^{*2/3} = \chi(z), \quad (\text{G15})$$

where $\chi(z)$ is given in Eq. (C10). From Eq. (D4) we know that $\chi(z)$ can be written in terms of the variable ϕ_2 as

$$\chi(z) = z^{2/3} \left(\frac{1}{2}\phi_2 + \frac{1}{\phi_2^2} \right). \quad (\text{G16})$$

The left-hand side of Eq. (G15) can be rewritten, using Eq. (G6), as

$$\frac{(z - y^*)^2}{4} + \frac{3}{2}y^{*2/3} = z^{2/3} \left[\frac{z^{4/3}}{4}(1 - \phi_2^{-3})^2 + \frac{3}{2}\phi_2^{-2} \right]. \quad (\text{G17})$$

Using Eq. (G11), we rewrite the term $z^{4/3}$ as

$$\frac{(z - y^*)^2}{4} + \frac{3}{2}y^{*2/3} = z^{2/3} \left[\frac{\phi_2^4(1 - \phi_2^{-3})^2}{2(\phi_2^3 - 1)} + \frac{3}{2}\phi_2^{-2} \right], \quad (\text{G18})$$

which can be rewritten, after few steps of algebra, as

$$\frac{(z - y^*)^2}{4} + \frac{3}{2}y^{*2/3} = z^{2/3} \left(\frac{1}{2}\phi_2 + \frac{1}{\phi_2^2} \right). \quad (\text{G19})$$

Recalling Eq. (G16), we finally obtain the result in Eq. (G15). Thus, we have shown that for any $z > 0$ the two representations of $F(z)$ in Eq. (18) and (G1) are equivalent.

Finally, we provide a physical interpretation of the formula in Eq. (G1). In the rest of this appendix we will only consider the case $X > 0$. We start from the definition of the PDF of X , given in Eq. (12),

$$P(X, N) = \prod_{i=1}^N \int_{-\infty}^{\infty} dx_i \mathcal{P}(x_i) \delta \left(X - \sum_{i=1}^N x_i \right), \quad (\text{G20})$$

where $\mathcal{P}(X)$ is the single-run PDF, given in Eq. (5). The expression in Eq. (G20), can be rewritten as

$$P(X, N) = \int_{-\infty}^{\infty} dx_1 \mathcal{P}(x_1) \quad (\text{G21})$$

$$\times \prod_{i=2}^N \int_{-\infty}^{\infty} dx_i \mathcal{P}(x_i) \delta \left(X - x_1 - \sum_{i=2}^N x_i \right).$$

Using Eq. (G20), we obtain

$$P(X, N) = \int_{-\infty}^{\infty} dx_1 \mathcal{P}(x_1) P(X - x_1, N - 1). \quad (\text{G22})$$

In the condensed phase, the term $\mathcal{P}(x_1)$ represents the condensate while the term $P(X - x_1, N - 1)$ is associated with the other $N - 1$ variables which are in the fluid phase, meaning that their contribution is of order one. Note that we have shown that no more than one condensate can appear in the thermodynamic limit (see App. F).

We now focus in the regime where $X \sim O(N^{3/4})$. Plugging the large deviation form of $P(X, N)$ in the fluid-phase, given in Eqs. (17) and (18), and the large- x behavior of $\mathcal{P}(x)$, given in Eq. (10), into Eq. (G22), we find

$$e^{-\sqrt{N}F(X/N^{3/4})} \sim \int_{-\infty}^{\infty} dx_1 e^{-(X-x_1)^2/(4N) - (3/2)|x_1|^{2/3}}. \quad (\text{G23})$$

Using the scaled variables $y = x_1/N^{3/4}$ and $z = X/N^{3/4}$, we obtain

$$e^{-\sqrt{N}F(z)} \sim \int_{-\infty}^{\infty} dy e^{-\sqrt{N}(z-y)^2/4 - (3/2)\sqrt{N}|y|^{2/3}}. \quad (\text{G24})$$

For large N , one can perform the integral over y via saddle-point approximation, yielding

$$F(z) = -\inf_{-\infty < y < \infty} \left[\frac{(z - y)^2}{4} + \frac{3}{2}|y|^{2/3} \right]. \quad (\text{G25})$$

Moreover, it is easy to show that configurations with $y < 0$ or $y > z$ are never optimal. Thus, we obtain

$$F(z) = \min_{0 \leq y \leq z} \left[\frac{(z-y)^2}{4} + \frac{3}{2}y^{2/3} \right], \quad (\text{G26})$$

in agreement with Eq. (G1).

Appendix H: Location of the condensate

In this Appendix, we derive an exact expression for the location y^* of the condensate, presented in Section IV. For $z > z_c$, we recall that $m_c = y^*/z$ is the fraction of the total displacement belonging to the condensate, where $z = XN^{-3/4}$. The variable y^* is defined as

$$y^* = \operatorname{argmin}_{y>0} [\psi_z(y)]. \quad (\text{H1})$$

where

$$\psi_z(y) = \frac{3}{2}y^{2/3} + F(z-y) - F(z), \quad (\text{H2})$$

and $F(z)$ is given in Eq. (64). We limit our discussion to the case $z > 0$, the complementary case $z < 0$ can be obtained by symmetry.

From Eq. (H1) we find that y^* satisfies the equation

$$\psi'_z(y^*) = 0, \quad (\text{H3})$$

where $\psi'_z(y)$ denotes the first derivative of $\psi_z(y)$ with respect to y . We now assume that $y^* > z - z_c$ (to be verified a posteriori). Under this assumption the condition in Eq. (H3) becomes

$$2y^{*-1/3} + y^* - z = 0. \quad (\text{H4})$$

Since y^* has to be a minimum, one also has the additional condition

$$\psi''_z(y^*) = -\frac{1}{3}y^{*-4/3} + \frac{1}{2} > 0, \quad (\text{H5})$$

where $\psi''_z(y)$ denotes the second derivative of $\psi_z(y)$ with respect to y .

Remarkably, it turns out that the solution y^* of the conditions above can be exactly related to the solution ϕ_2 of the saddle-point equation (D3) as

$$y^* = z \phi_2^{-3}. \quad (\text{H6})$$

Thus, from the results in Appendix C, we know that no solution of the saddle-point equation exists for $z < z_\ell = 4(2/3)^{3/4}$. Thus, for $z < z_\ell$ the function $\psi_z(y)$ will not have any minimum for $y > 0$ and no condensation is possible. For $z > z_\ell$ a minimum of the function $\psi_z(y)$ appears at $y = y^* > 0$. However, it is easy to check that, for $z_\ell < z < z_c$, this minimum will correspond to a non-zero value of the function $\psi_z(y^*)$ and thus the probability density of configurations with $y > 0$ will decay exponentially fast with N [see Eq. (82)]. Finally, above the transition $\psi_z(y^*)$ becomes, using Eq. (64),

$$\psi_z(y^*) = \frac{3}{2}y^{*2/3} + \frac{(z-y^*)^2}{4} - \chi(z), \quad (\text{H7})$$

where $\chi(z)$ is defined in Eq. (C4). We recall that the function $\chi(z)$ can be expressed in terms of the variable ϕ_2 , as given in Eq. (D4). Using also the representation of y^* in terms of ϕ_2 , given in Eq. (H6), we obtain

$$\begin{aligned} \psi_z(y^*) & \\ &= \frac{3}{2}z^{2/3}\phi_2^{-2} + z^2 \frac{(1-\phi_2^{-3})^2}{4} - z^{2/3} \left(\frac{1}{2}\phi_2 + \phi_2^{-2} \right). \end{aligned} \quad (\text{H8})$$

From Eq. (D3), we obtain

$$z^{4/3} = \frac{2\phi_2^4}{\phi_2^3 - 1}. \quad (\text{H9})$$

Thus, writing the term z^2 in Eq. (H9) as $z^2 = z^{2/3} z^{4/3}$ and using Eq. (H9), we obtain, after few steps of algebra, that for $z > z_c$ (see also Fig. 4)

$$\psi_z(y^*) = 0. \quad (\text{H10})$$

Thus, for $z > z_c$ a condensate appears at $x = y^*N^{3/4}$ [see Eq. (82)].

It is also possible to find an explicit expression for y^* . Solving the conditions in Eqs. (H3) and (H5), we obtain

$$\begin{aligned} y^* &= z \left(\frac{z^{4/3}}{8} + \frac{1}{8} \left(\frac{64(2/3)^{1/3}}{a(z)} + 4(2/3)^{2/3} a(z) z^{4/3} + z^{8/3} \right)^{1/2} - \frac{1}{2} \left(-\frac{4(2/3)^{1/3}}{a(z)} - \frac{a(z)z^{4/3}}{2 \cdot 2^{1/3} 3^{2/3}} + \frac{z^{8/3}}{8} \right. \right. \\ &\left. \left. + \frac{z^4}{8 \sqrt{\frac{64(2/3)^{1/3}}{a(z)} + 4 \left(\frac{2}{3} \right)^{2/3} a(z) z^{4/3} + z^{8/3}}} \right)^{1/2} \right)^{-3}, \end{aligned} \quad (\text{H11})$$

where

$$a(z) = \left(9 + \sqrt{3} \sqrt{27 - \frac{2048}{z^2}} \right)^{1/3}. \quad (\text{H12})$$

From this expression in Eq. (H11), we obtain, for $z = z_c = 2^{7/4}$, $y^* = 2^{3/4}$ and hence that $m_c = y^*/z = 1/2$, as given in the first line of Eq. (86). It is easy to show that y^* is an increasing function of z and that our assumption $y^* > z - z_c$ is always satisfied. Moreover, close to $z = z_c$, we find that

$$y^* \simeq 2^{3/4} + \frac{3}{2}(z - z_c), \quad (\text{H13})$$

and thus that

$$m_c \simeq \frac{1}{2} + \frac{z - z_c}{2^{7/4}}. \quad (\text{H14})$$

Finally, to investigate the large- z behavior of y^* , we use express y^* in terms of the variable ϕ_2 , using Eq. (H6). Using the asymptotics of ϕ_2 for large z , given in Eq. (D5), we obtain

$$y^* \simeq z - 2z^{-1/3}, \quad (\text{H15})$$

and, using $m_c = h^*/z$, we finally find that, for large z

$$m_c \simeq 1 - 2z^{-4/3}, \quad (\text{H16})$$

as given in the second line of Eq. (86).

Appendix I: Shape of the condensate

In Section IV we have shown that for $z > z_c$ the condensate appears as a bump in the marginal probability $p(x|X)$ of the single displacement x conditioned on the total displacement X . We have also shown that the condensate is located in the proximity of $x = y^*N^{3/4}$, where the function $p(x|X)$ can be approximated as

$$\begin{aligned} p(x|X) &\simeq p_{\text{cond}}(x - y^*N^{3/4}, N) \\ &\sim \exp \left[-\frac{1}{2} \psi_z''(y^*) \frac{(x - y^*N^{3/4})^2}{N} \right], \end{aligned} \quad (\text{I1})$$

where y^* is given in Eq. (H11) and $\psi_z''(y^*)$ is given in Eq. (H5). The goal of this appendix is to compute the full distribution $p_{\text{cond}}(y, N)$ (and not only the exponential part given above). Knowing the full expression of the function $p_{\text{cond}}(y, N)$ is useful because the integral

$$\int_{-\infty}^{\infty} dy p_{\text{cond}}(y, N) \quad (\text{I2})$$

is the probability that a specific displacement among x_1, \dots, x_N becomes the condensate. In the presence of a single condensate one expects this probability to be $1/N$.

Our starting point is the exact expression in Eq. (73), which reads

$$p(x|X) = \mathcal{P}(x) \frac{P(X - x, N - 1)}{P(X, N)}. \quad (\text{I3})$$

We are interested in the regime where $x = yN^{3/4}$ and $X = zN^{3/4}$, the variables y and z being of order one. Note that the function $P(X, N)$ has different expressions below and above the transition. Since $z > z_c$ the term $P(X, N)$ is given by [see Eq. (C4)]

$$P(X, N) \simeq \frac{1}{-s_2 \sqrt{-G_z''(s_2)}} N^{3/4} e^{-\sqrt{N} G_z(s_2)}. \quad (\text{I4})$$

where

$$G_z(s_2) = z s_2 + s_2^2 - \frac{1}{2s_2^2}, \quad (\text{I5})$$

and

$$G_z''(s_2) = 2 - \frac{3}{s_2^4} < 0. \quad (\text{I6})$$

We recall that the variable s_2 is the largest negative solution of the saddle point equation (C3) and that it is related to the variable ϕ_2 by $s_2 = -z^{-1/3}\phi_2$.

In Appendix H we have shown that the condensate is located at $y = y^*$ and that $y^* > z - z_c$, thus $P(X - x, N - 1)$ is given by the Gaussian weight (see Eq. (56))

$$P(X - x, N - 1) \simeq \frac{1}{2\sqrt{\pi N}} e^{-\sqrt{N}(z-y)^2/4}. \quad (\text{I7})$$

Finally, we can approximate $\mathcal{P}(x)$, using the expansion in Eq. (10), as

$$\mathcal{P}(x = yN^{3/4}) \approx \frac{N^{-1/4}}{\sqrt{3}y^{1/3}} e^{-\frac{3}{2}\sqrt{N}y^{2/3}}. \quad (\text{I8})$$

Thus, plugging the expressions in Eqs. (I4), (I7), and (I8), into Eq. (I3), we obtain

$$\begin{aligned} p(x|X) &\simeq \frac{-s_2 \sqrt{-G_z''(s_2)}}{\sqrt{3\pi}y^{1/3}} \\ &\times \exp \left[-\sqrt{N} \left(\frac{3}{2}y^{2/3} + (z - y)^2/4 - G_z(s_2) \right) \right]. \end{aligned} \quad (\text{I9})$$

To investigate the shape of the condensate, we now expand the expression (I10) around y^* , the location of the condensate. Thus, setting $x = N^{3/4}(y^* + wN^{-1/4})$ (with w of order one) and expanding for large N we obtain

$$\begin{aligned} p(x|X) &\simeq p_{\text{cond}}(\sqrt{N}w, N) = \frac{-s_2 \sqrt{-G_z''(s_2)}}{2\sqrt{3\pi}y^{*1/3}} \\ &\times \exp \left[-\frac{1}{2} \psi_z''(y^*) w^2 \right], \end{aligned} \quad (\text{I10})$$

where $\psi_z''(y)$ is given in Eq. (H5).

We can now compute the integral of the condensate distribution $p_{\text{cond}}(x, N)$. Using the expression in Eq. (I11) with $w = N^{-1/2}(x - N^{3/4}y)$ we obtain

$$\int_{-\infty}^{\infty} dx p_{\text{cond}}(x, N) = \frac{1}{\sqrt{6}} \frac{-s_2 \sqrt{-G_z''(s_2)}}{y^{*1/3} \sqrt{\psi_z''(y^*)}}. \quad (\text{I11})$$

It is useful to write the right-hand side of this equation in terms of the variable ϕ_2 , defined in Appendix C as the smallest positive root of Eq. (D3). Indeed, using the relations $y^* = z\phi_2^{-3}$ and $s_2 = -z^{-1/3}\phi_2$, we obtain

$$\int_{-\infty}^{\infty} dx p_{\text{cond}}(x, N) = \frac{1}{\sqrt{6}} z^{-2/3} \phi_2^2 \frac{\sqrt{-G_z''(-z^{-1/3}\phi_2)}}{\sqrt{\psi_z''(z\phi_2^{-3})}} \frac{1}{N}. \quad (\text{I12})$$

Using the expressions for $G_z''(s)$ and $\psi_z''(s)$, given in Eqs. (I6) and (H5), we obtain

$$\int_{-\infty}^{\infty} dx p_{\text{cond}}(x, N) = \frac{1}{\sqrt{6}} \frac{\sqrt{3 - 2z^{-4/3}\phi_2^4}}{\sqrt{1/2 - z^{-4/3}\phi_2^4/3}} \frac{1}{N} = \frac{1}{N}, \quad (\text{I13})$$

as anticipated in Eq. (91). This result implies that the condensate is localized in just one of the displacements x_1, \dots, x_N .

-
- [1] S. Ramaswamy, *Annu. Rev. Condens. Matter Phys.* **1**, 323 (2010).
- [2] T. Vicsek, A. Czirók, E. Ben-Jacob, I. Cohen, and O. Shochet, *Phys. Rev. Lett.* **75**, 1226 (1995).
- [3] T. Vicsek and A. Zafeiris, *Phys. Rep.* **517**, 71 (2012).
- [4] R. Nitzan, R. Voituriez, and N. S. Gov, *Phys. Rev. E* **99**, 022419 (2019).
- [5] J. Tailleur, M. E. Cates, *Phys. Rev. Lett.* **100**, 218103 (2008).
- [6] M. E. Cates, *Rep. Prog. Phys.* **75**, 042601 (2012).
- [7] H. C. Berg, *E. coli in Motion* (Springer, 2014).
- [8] M. E. Cates, J. Tailleur, *Annu. Rev. Condens. Matter Phys.* **6**, 219-244 (2015).
- [9] C. Bechinger, R. Di Leonardo, H. Löwen, C. Reichhardt, G. Volpe, and G. Volpe, *Rev. Mod. Phys.* **88**, 045006 (2016).
- [10] F. Mori, P. Le Doussal, S. N. Majumdar, and G. Schehr, *Phys. Rev. Lett.* **124**, 090603 (2020).
- [11] F. Mori, P. Le Doussal, S. N. Majumdar, and G. Schehr, *Phys. Rev. E*, **102**, 042133 (2020).
- [12] B. De Bruyne, S. N. Majumdar, and G. Schehr, *J. Stat. Mech.* 043211 (2021).
- [13] M. Kac, *Rocky Mountain J. Math.* **4**, 497 (1974).
- [14] W. Stadje, *J. Stat. Phys.* **46**, 207 (1987).
- [15] E. Orsingher, *Stoch. Process. Their Appl.* **34**, 49 (1990).
- [16] G. H. Weiss, *Physica A* **311**, 381 (2002).
- [17] P. Hänggi and P. Jung, *Adv. Chem. Phys.* **89**, 239 (1995).
- [18] J. Masoliver and K. Lindenberg, *Eur. Phys. J. B* **90**, 1 (2017).
- [19] A. P. Solon, Y. Fily, A. Baskaran, M. E. Cates, Y. Kafri, M. Kardar, and J. Tailleur, *Nature Phys.* **11**, 673 (2015).
- [20] A. Dhar, A. Kundu, S. N. Majumdar, S. Sabhapandit, G. Schehr, *Phys. Rev. E* **99**, 032132 (2019).
- [21] F. J. Sevilla, A. V. Arzola, E. P. Cital, *Phys. Rev. E* **99**, 012145 (2019).
- [22] E. Mallmin, R. A. Blythe, M. R. Evans, *J. Stat. Mech.* 013204 (2019).
- [23] U. Basu, S. N. Majumdar, A. Rosso, S. Sabhapandit, G. Schehr, *J. Physics A: Math. Theor.* **53**, 09LT01 (2020).
- [24] K. Martens, L. Angelani, R. Di Leonardo, and L. Bocquet, *Eur. Phys. J. E* **35**, 84 (2012).
- [25] A. De Gregorio, and C. Macci, *Stat. Prob. Lett.* **82**, 1874 (2012).
- [26] G. Gradenigo, and S. N. Majumdar, *J. Stat. Mech.* 053206 (2019).
- [27] I. Santra, U. Basu, and S. Sabhapandit, *Phys. Rev. E* **101**, 062120 (2020).
- [28] K. Proesmans, R. Toral, and C. Van den Broeck, *Physica A* **552**, 121934 (2020).
- [29] F. Mori, P. Le Doussal, S. N. Majumdar, and G. Schehr, *Phys. Rev. E* **103**, 062134 (2021).
- [30] M. R. Evans and T. Hanney, *J. Phys. A: Math. Gen.* **38**, R195 (2005).
- [31] S. N. Majumdar, Real-space condensation in stochastic mass transport models. *Exact Methods in Low-dimensional Statistical Physics and Quantum Computing: Lecture Notes of the Les Houches Summer School: Volume 89, July 2008, 407* (2010).
- [32] K. Ø. Rasmussen, T. Cretegnny, P. G. Kevrekidis, and N. Gronbech-Jensen, *Phys. Rev. Lett.* **84**, 3740 (2000).
- [33] Iubini, Stefano, Antonio Politi, and Paolo Politi, *J. Stat. Mech.* 073201 (2017).
- [34] G. Gradenigo, S. Iubini, R. Livi, and S. N. Majumdar, *J. Stat. Mech.* 023201 (2021).
- [35] G. Gradenigo, S. Iubini, R. Livi, and S. N. Majumdar, *Eur. Phys. J. E* **44**, 1 (2021).
- [36] G. Gotti, S. Iubini, and P. Politi, *Phys. Rev. E* **103**, 052133 (2021).
- [37] J-P. Bouchaud, and M. Mézard, *Physica A* **282**, 536-545 (2000).
- [38] Z. Burda, D. Johnston, J. Jurkiewicz, M. Kamiński, M. A. Nowak, G. Papp, and I. Zahed, *Phys. Rev. E* **65**, 026102 (2002).
- [39] M. Filiasi, E. Zarinelli, E. Vesselli, and M. Marsili, preprint arXiv:1309.7795 (2013).
- [40] S. N. Majumdar, M. R. Evans, and R. K. P. Zia, *Phys. Rev. Lett.* **94**, 180601 (2005).
- [41] M. R. Evans, S. N. Majumdar, and R. K. P. Zia, *J. Stat. Phys.* **123**, 357 (2006).
- [42] M. R. Evans, T. Hanney, and S. N. Majumdar, *Phys. Rev. Lett.* **97**, 010602 (2006).
- [43] M. R. Evans and S. N. Majumdar, *J. Stat. Mech.* 05004 (2008).
- [44] M.R. Evans, S. N. Majumdar, I. Pagonabarraga, and E.

- Trizac, J. Chem. Phys. **132**, 014102 (2010).
- [45] J. Szavits-Nossan, M. R. Evans, and S. N. Majumdar, Phys. Rev. Lett. **112**, 020602 (2014).
- [46] J. Szavits-Nossan, M. R. Evans, and S. N. Majumdar, J. Phys. A: Math. Theor. **47**, 455004 (2014).
- [47] J. Szavits-Nossan, M. R. Evans, and S. N. Majumdar, J. Phys. A: Math. Theor. **50**, 024005 (2016).
- [48] G. Gradenigo, and E. Bertin, Entropy **19**, 517 (2017).
- [49] W. Feller, *Introduction to Probability Theory and Its Applications*, John Wiley & Sons, New York (1950).
- [50] M. Höll, and E. Barkai, preprint arXiv:2106.14222 (2021).
- [51] A. V. Nagaev, Theory of Probability & Its Applications **14**, 51 (1969).
- [52] A. V. Nagaev, Theory of Probability & Its Applications **14**, 193 (1969).
- [53] F. Brosset, T. Klein, A. Lagnoux, and P. Petit, preprint arXiv:2007.08164 (2020).
- [54] P. Embrechts, C. Klppelberg, and T. Mikosch, *Modeling Extremal Events for Insurance and Finance* (Springer, Berlin, 1997).
- [55] A. Vezzani, E. Barkai, and R. Burioni, Phys. Rev. E **100**, 012108 (2019).
- [56] S. N. Majumdar, A. Pal, and G. Schehr, Phys. Rep. **840**, **1** (2020).
- [57] M. R. Evans, and S. N. Majumdar, Phys. Rev. Lett. **106**, 160601 (2011).
- [58] M. R. Evans, S. N. Majumdar, and G. Schehr, J. Phys. A.: Math. Theor. **53**, 193001 (2020).
- [59] C. Nadal, S. N. Majumdar, and M. Vergassola, Phys. Rev. Lett. **104**, 110501 (2010).
- [60] C. Nadal, S. N. Majumdar, and M. Vergassola, J. Stat. Phys. **142**, 403-438 (2011).